

## Chapter - IV

# Effect of swift heavy ions on physical properties of PMMA/Cu and PS/Cu nanocomposites

---

### Abstract

*Effect of swift heavy ions (120 MeV Si ions, 85 MeV C ions) induced modifications of Copper nanoparticles dispersed PMMA and PS nanocomposites films at different fluences were studied. 120 MeV Si swift heavy ions induced more prominent effects on the physico-chemical properties of polymer nanocomposites compared to those of C-ions. An XRD analysis reveals that the crystallite size of the composites decreased after ion beam irradiation which is also corroborated by the DSC analysis due to the chain scissioning upon irradiation in PMMA nanocomposites. In PS nanocomposites, we observed cross linking upon irradiation. It was observed from the UV- visible spectroscopy analysis that the band gap value moved to the lower energy on doping with metal nanoparticles, as well as upon irradiation. SEM images showed damages upon ion beam irradiation. The dielectric constant of the composites increased with the increase of metal content. These phenomena could be interpreted from interfacial polarization of heterogeneous systems.*

#### 4.0 Introduction:

Polymers have traditionally been considered as excellent host matrices for composite materials. Several advanced polymer composites have been synthesized with a wide variety of inclusions like metals, semiconductors, carbon nanotubes and magnetic nanoparticles [1–3]. Many attractive properties of polymers like non-corrosiveness, light weight, mechanical strength and dielectric tenability can be utilized along with magnetic and optical properties of nanoparticles to make multifunctional materials. Inclusion of nanoparticles exhibit novel properties that significantly differ from those of corresponding bulk solid state owing to the different effects in terms of the small size effect, surface effect, quantum size effect and macroscopic quantum tunnel effect [4–6]. Copper nanoparticles have potential applications as fillers in polymers in many electronic devices. The progress in miniaturized nano devices that integrate electronic, photonic, chemical, and/or biological features is important for electronic as well as sensing devices [7].

Ion beam irradiation of polymeric materials can induce irreversible changes in their macroscopic properties, such as, electrical, thermal and surface related mechanical properties. These changes are responsible to fundamental events like electronic excitation, ionization, chain scission and cross-linking as well as mass loss, which take place due to ion beam irradiation [8].

In this chapter we are dealt with polymer nanocomposites and effect of irradiation upon

(i) PMMA + Cu [9]

(ii) PS + Cu [10]

Properties and preparation methods of nanocomposites have been discussed in chapter 2. All the films were irradiated with 120 MeV Si- ions and 85 MeV C- ions at the

fluences of  $1 \times 10^{11}$ ,  $1 \times 10^{12}$  ions/cm<sup>2</sup> at Inter University Accelerator Centre (IUAC), New Delhi, India. We have studied changes in the structural, thermal, optical and dielectric properties of composites due to swift heavy ion irradiation by means of X-ray diffraction, differential scanning calorimetry, UV-visible spectroscopy and impedance gain phase analyzer.

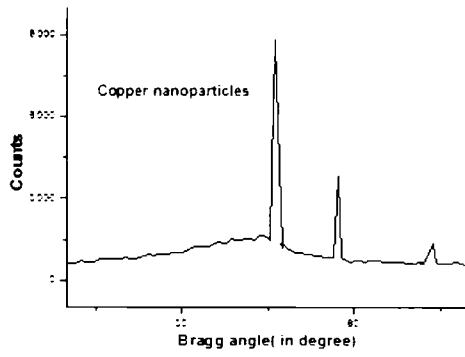
#### **4.1 Effect of swift heavy ions irradiation on PMMA + Cu nanocomposites:**

##### ***4.1.1 X-ray diffraction analysis:***

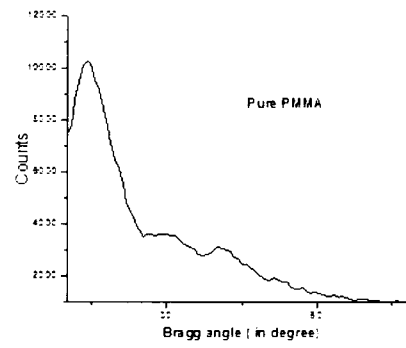
Fig. 4.1(a-g) shows XRD spectra of the copper nanocomposite films, which illustrate the amorphous nature of PMMA and the crystalline behavior of copper nanoparticles. The average particle size of the copper nanoparticles was obtained around 10.81 nm. The diffraction patterns of the irradiated samples by 85 MeV C ions and 120 MeV Si ions exhibited decrease in the peak intensity and an increase in the full width at half maximum (FWHM) corresponding to all observed peaks of copper. This behavior may be attributed to chain scissioning taking place, which may results in the alignment of the polymeric chains. The average crystallite size ( $t$ ) for pristine and irradiated samples was calculated using Scherrer's formula [11] as dicussed in chapter 2 in section 2.3.1 from the realtion 2.2.3.

$$b = K\lambda/L\cos\theta$$

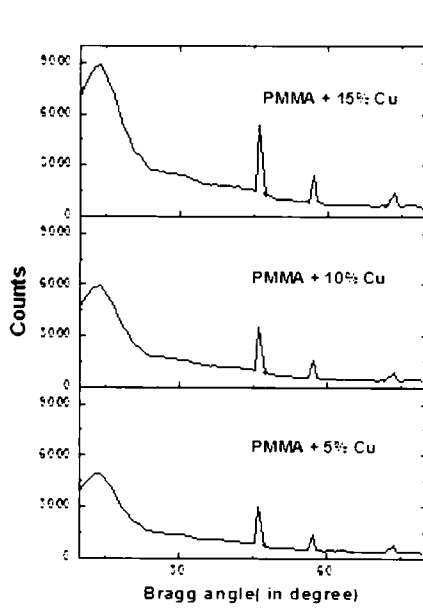
where  $b$  is FWHM in radians,  $\lambda$  is the wavelength of X-ray beam (1.5418 Å),  $L$  is the crystallite size in Å,  $\theta$  is the angle between the atomic plane and both the incident and reflected planes,  $K$  is a constant which varies from 0.89 to 1.39, but for most of the cases it is close to 1.



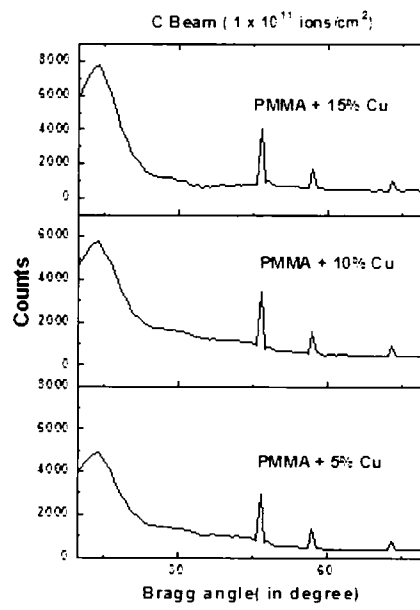
(a)



(b)



(c)



(d)

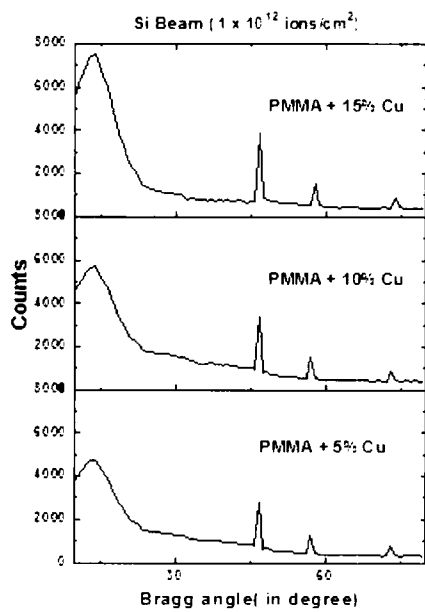
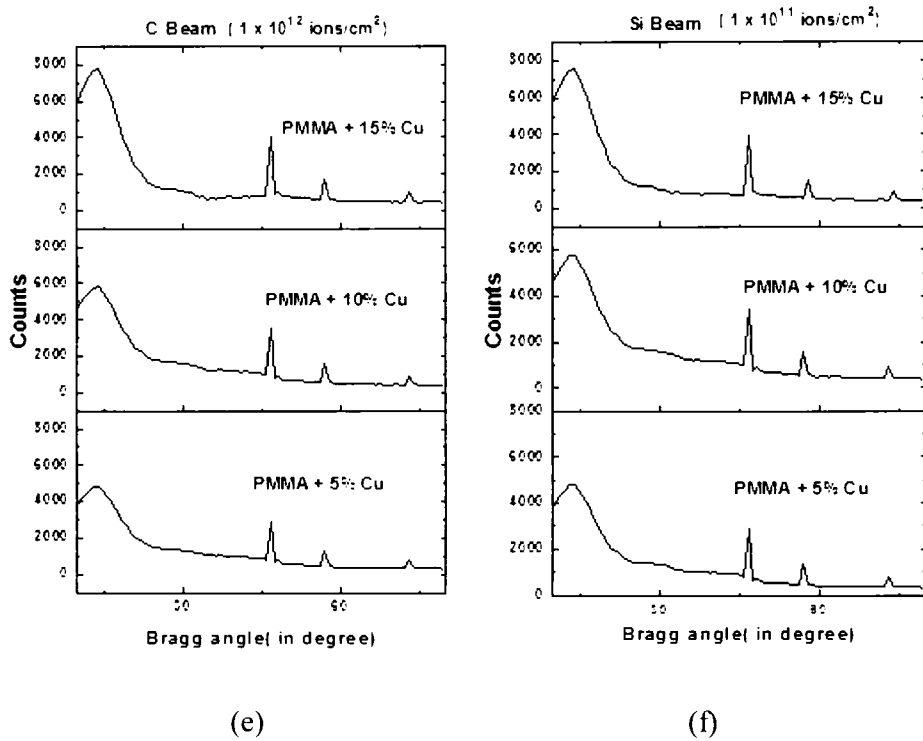


**Fig. 4.1 X-ray diffraction patterns of (a) copper nanoparticles (b) pure PMMA (c) PMMA+ Cu (pristine) (d) C beam ( $1 \times 10^{11}$  ions/cm<sup>2</sup>) (e) C beam ( $1 \times 10^{12}$  ions/cm<sup>2</sup>) (f) Si beam ( $1 \times 10^{11}$  ions/cm<sup>2</sup>) (g) Si beam ( $1 \times 10^{12}$  ions/cm<sup>2</sup>)**

The crystallite size was calculated corresponding to the peak of the pristine and irradiated samples and the results are listed in Table 4.1 [12]. Irradiation deposited

large amount of energy in material and leads to decrease in crystallite size. This may be attributed to splitting of crystalline grains. The decrease in crystallite size suggested the chain scissioning mechanism.

**Table 4.1 Crystallite size of pristine and irradiated samples**

Sample	Pristine		C Beam		Si Beam	
	2 $\theta$	Crystallite size (nm)	Crystallite size (nm) ( $1 \times 10^{11}$ ) ions/cm <sup>2</sup>	Crystallite size (nm) ( $1 \times 10^{12}$ ) ions/cm <sup>2</sup>	Crystallite size (nm) ( $1 \times 10^{11}$ ) ions/cm <sup>2</sup>	Crystallite size (nm) ( $1 \times 10^{12}$ ) ions/cm <sup>2</sup>
PMMA+ 5%Cu	46.73	12.16	11.64	11.26	11.56	11.21
	58.05	12.64	11.61	11.14	11.20	11.08
	Average	12.40	11.63	11.2	11.38	11.15
PMMA + 10%Cu	46.56	12.23	11.78	11.56	11.48	10.86
	58.05	12.89	11.51	11.34	11.16	10.58
	Average	12.56	11.65	11.45	11.32	10.72
PMMA + 15%Cu	46.39	12.36	11.81	11.68	11.11	10.54
	58.01	12.24	11.25	11.22	10.89	10.39
	Average	12.30	11.53	11.45	11.00	10.47

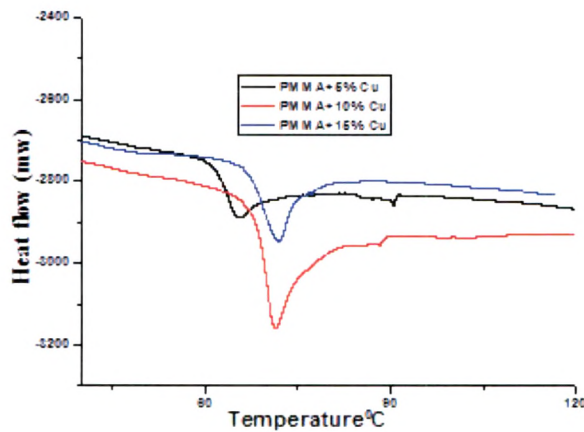
#### 4.1.2 Thermal response (Differential scanning calorimetry (DSC)):

A differential scanning calorimetry experiment was performed using a reference material, and a predetermined heating (or cooling) rate was imposed to the system with a temperature excursion. The sample followed the temperature of the reference, and the heating power difference between the sample and reference was recorded. The values of  $T_g$  were taken as the midpoint of the glass transition event and collected as shown in Fig. 4.2. The pure PMMA has a  $T_g$  value of 64.60°C, while the tendency of increase in  $T_g$  value after insertion of copper nanoparticles was observed for Cu/PMMA nanocomposites. We found the value of  $T_g$  for pristine and irradiated samples at 71.89°C and 61.8°C, respectively, for the highest concentration of copper.

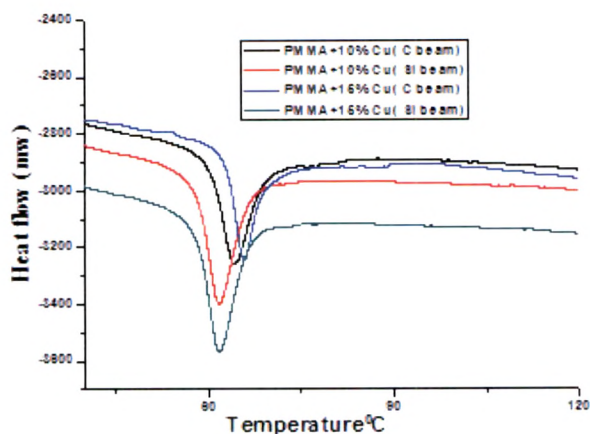
The value of  $T_g$  for highest fluence is listed in Table 4.4. The results reveal that the glass transition temperature increases for the composites as compared with the pure PMMA and may be due to the interactions of the filler nanoparticles and PMMA in a more ordered state and resulting in the cross-linking of the polymer and nanoparticles. After irradiation, it was found that  $T_g$  shifted to lower temperature. It reveals that the ion irradiation leads to polymer chain scissioning and a subsequent reduction in the molecular weight. As a result, the system moved toward the more disordered state, which is also corroborated with XRD results [13].

**Table 4.2 Values of glass transition for pristine and irradiated composites**

Sample name	$T_g$ (Pristine)	$T_g$ (C beam)	$T_g$ (Si beam)
PMMA + 10 %Cu	70.2	65.7	64.2
PMMA + 15 %Cu	71.9	61.8	61.5



(a)

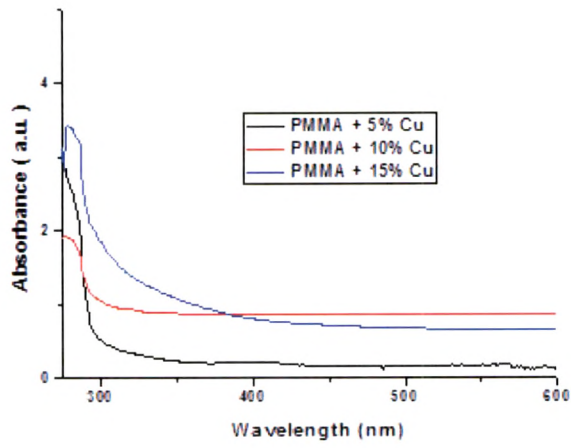


(b)

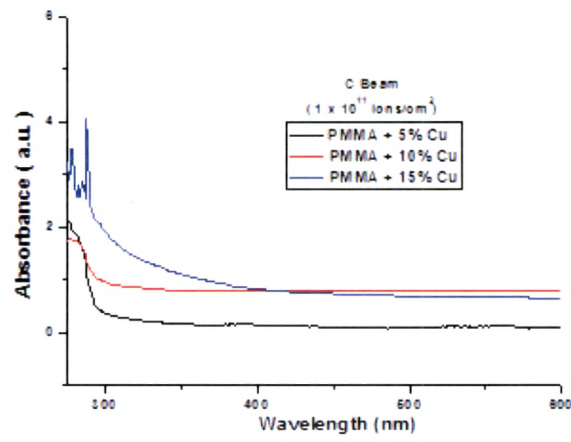
**Fig. 4.2 DSC spectra of (a) composites (b) irradiated films ( $1 \times 10^{12}$  ions/cm<sup>2</sup>)**

#### **4.1.3 Optical response:**

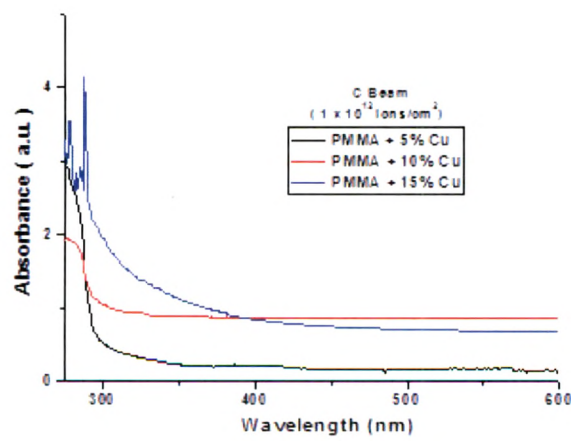
The promotion of electrons in the  $\sigma$ ,  $\pi$  and  $n$  orbitals from ground state to the higher energy states which are described by molecular orbitals due to the absorption of light energy by polymeric samples in the UV and visible regions. Many of the optical transitions which occur due to the presence of impurities have energies in the visible region of the spectrum, consequently the defects are referred to as colour centres. The effect of ion beam interaction with polymers produces damage and leads to the generation of new defects and charge states [14, 15]. A shift in the absorption edge towards longer wavelength is observed for irradiated samples. This behaviour is generally interpreted as caused by the formation of extended systems of conjugated bonds, i.e. possible formation of carbon clusters. In the investigated range of wavelengths the absorption bands are associated to the  $\pi$ - $\pi^*$  electronic transitions. These types of transitions occur in the unsaturated centers of the molecules, i.e. in compounds containing double or triple bonds and also in aromatics. The excitation of  $\pi$  electron requires smaller energy and hence, transition of this type occurs at longer wavelengths [16].



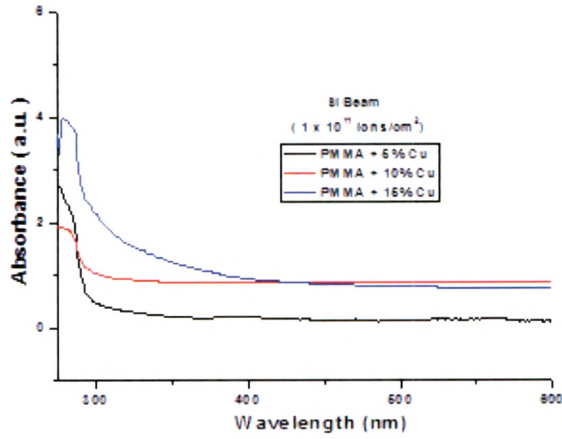
(a)



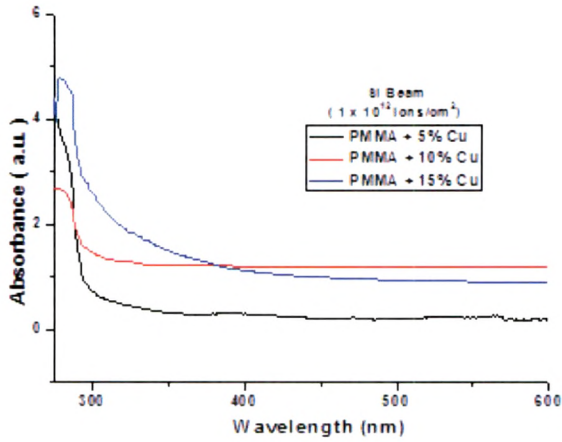
(b)



(c)



(d)



(e)

**Fig. 4.3 Absorbance spectra for (a) PMMA+ Cu( pristine) (b) C beam ( $1 \times 10^{11}$  ions/cm<sup>2</sup>) (c) C beam ( $1 \times 10^{12}$  ions/cm<sup>2</sup>) (d) Si beam ( $1 \times 10^{11}$  ions/cm<sup>2</sup>) (e) Si beam ( $1 \times 10^{12}$  ions/cm<sup>2</sup>)**

***Determinations of band gap:***

The change in optical properties has been studied by Perkin- Elmer 25 Lambda UV-Visible spectrophotometer for the pristine and irradiated samples in the frequency range 200-800 cm<sup>-1</sup>. The optical band gap  $E_g$  is obtained by Tauc’s equation [17] as explained in chapter 2 in section 2.3.3 by relation 2.2.4.

$$\omega\varepsilon(\lambda)=(\hbar\omega-E_g)^2$$

where  $\varepsilon(\lambda)$  is the optical absorbance and  $\lambda$  is the wavelength. The intersection of the extrapolated spectrum with the abscissa of the plot  $\varepsilon^{1/2}/\lambda$  versus  $1/\lambda$  yields the gap wavelength  $\lambda_g$  from which the energy gap is derived as  $E_g = hc/\lambda_g$ . It is noticed that the band gap (energy gap) value shifted to lower energy from 4.30 eV upto 3.22 eV due to doping of copper nanoparticles and also upon irradiation. This is because of the scissioning of polymer chain and as a result, creation of free radicals, unsaturation etc. and thus a capability of increasing the conductivity of the composites [18].

**Table 4.3 Band gap (B.G) and no. of carbon atoms (N) of pristine and irradiated samples**

Sample	Pristine	C Beam		Si Beam	
	B.G eV	B.G eV $1 \times 10^{11}$ ions/cm <sup>2</sup>	B.G eV $1 \times 10^{12}$ ions/cm <sup>2</sup>	B.G eV $1 \times 10^{11}$ ions/cm <sup>2</sup>	B.G eV $1 \times 10^{12}$ ions/cm <sup>2</sup>
PMMA + 5%Cu	4.30	4.24	4.13	4.12	4.10
PMMA + 10%Cu	4.11	4.05	3.95	3.80	3.62
PMMA + 15%Cu	3.78	3.65	3.55	3.40	3.22

Sample	Pristine	C Beam		Si Beam	
	No. of carbon atoms(N)	No. of carbon atoms(N) $1 \times 10^{11}$ ions/cm <sup>2</sup>	No. Of carbon atoms(N) $1 \times 10^{12}$ ions/cm <sup>2</sup>	No. of carbon atoms(N) $1 \times 10^{11}$ ions/cm <sup>2</sup>	No. Of carbon atoms(N) $1 \times 10^{12}$ ions/cm <sup>2</sup>
PMMA + 5%Cu	67	68	69	69	70
PMMA + 10%Cu	72	73	75	84	90
PMMA + 15%Cu	82	85	90	93	113

The number of carbon atoms per cluster (N) can be calculated by following the relation 2.2.5 [12] given in chapter 2; the values of are listed in Table 4.3.

$$E_g = 34.3/\sqrt{N} \text{ eV}$$

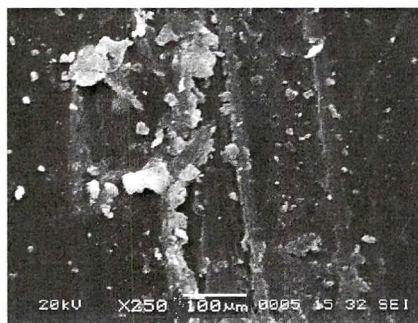
where N is the number of carbon atoms per cluster and  $E_g$  is the energy band gap.

#### 4.1.4 Surface morphology:

Fig. 4.4(a–d) shows the SEM images of pristine, composites and irradiated composite films at a fluence of  $1 \times 10^{12}$  ions/cm<sup>2</sup> with magnification of X250. The analysis shows that the filled partilces are distributed randomly in the matrix which display continuous contact between themselves and formed conducting paths. After irradiation, significant changes in surface morphology were observed. Considerable damage in the polymeric structure was observed after irradiation, which is also responsible for decrease in crystallinity of the material as indicated by XRD analysis [19].



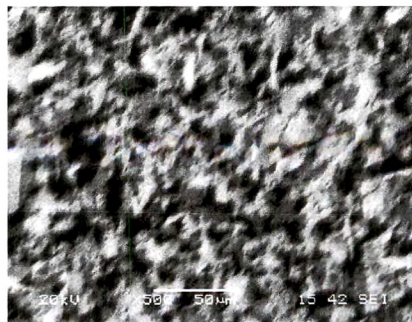
(a)



(b)



(c)



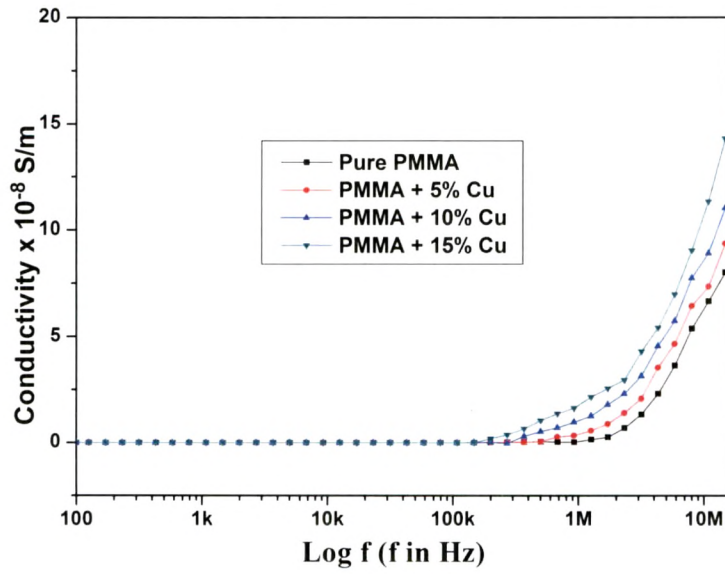
(d)

**Fig. 4.4 SEM images of (a) PMMA+ 15 % Cu (pristine) (b) PMMA + 15 % Cu (C beam) (c) PMMA + 15 % Cu (Si beam) and (d) Copper nanoparticles**

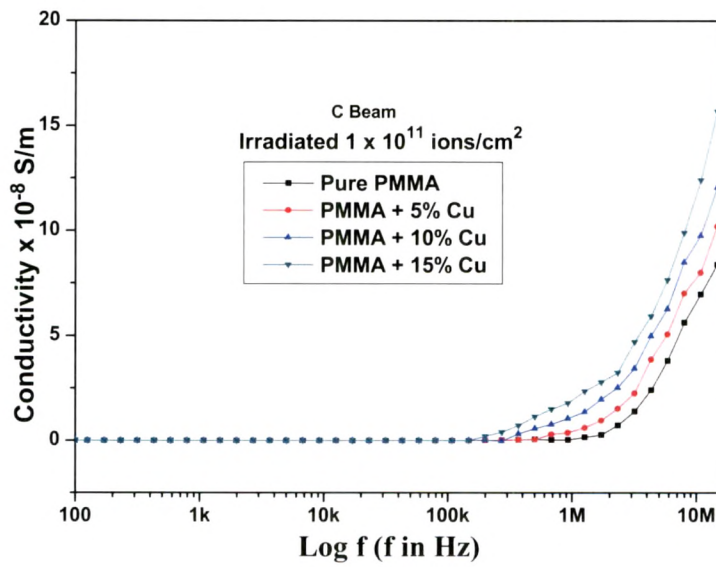
#### ***4.1.5 AC Electrical Frequency Response:***

*Conductivity:* AC electrical measurement was carried out for pristine and irradiated samples. Fig. 4.5 (a-e) shows the variation of conductivity with log of frequency for the pristine and irradiated samples at different copper nanoparticles concentrations. The increase in conductivity with copper nanoparticles concentration for pristine samples may be attributed to the conductive phase formed by dispersed copper nanoparticles in polymer matrix [20–22]. As shown in Fig. 4.5(a-e), we observed two behaviors (i) the frequency independent conductivity in the region of 100 Hz to 1 MHz which is due to free charge carriers available in the composite system and (ii) the frequency dependent conductivity in the region of 1–10 MHz because of trapped charges, which are active at higher frequency only and it contributed to sudden rise in conductivity [23]. The electrical conduction in pure PMMA may occur by the electron jumping (hopping or tunnelling) between filled and empty sites localized in the energy band gap due to the presence of carbonyl group (C=O) in PMMA which may be acted as an electron donor group at higher frequency range [24]. The increase in conductivity is related to a possible increase in the number of conduction paths created between the filler (copper nanoparticles) particles aggregates in the composite and as a consequence electrical path in the polymer matrix due to a decrease in the width of the potential barriers within the bulk region of composites. Therefore, more charge carriers may be able to ‘hop’ by tunnelling, resulting in the increase in the bulk conductivity and it also increases with increasing filler concentrations [25]. Irradiation is expected to promote the metal to polymer bonding and convert polymeric structure

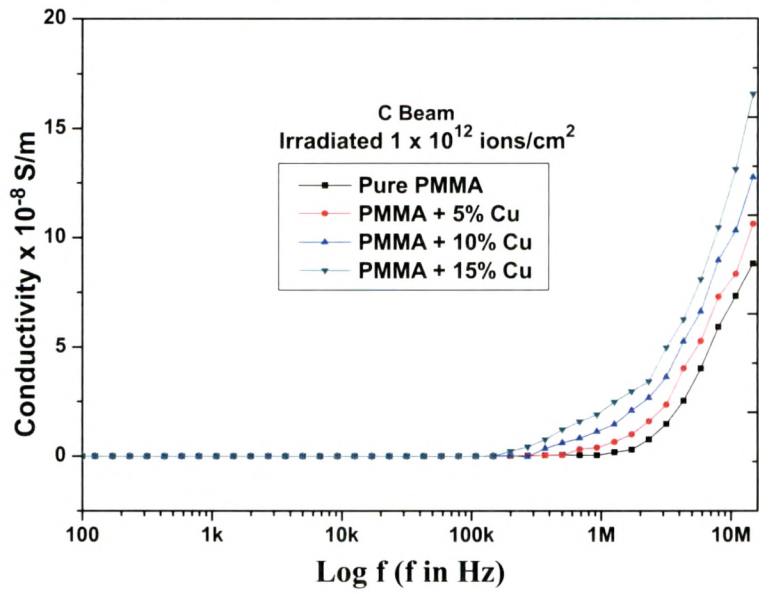
into hydrogen depleted carbon network that is believed to make the polymer more conductive [26].



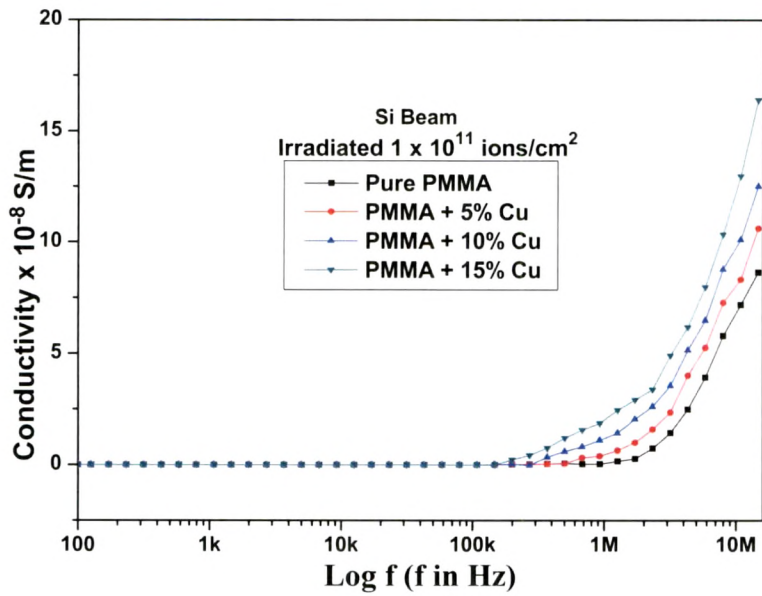
(a)



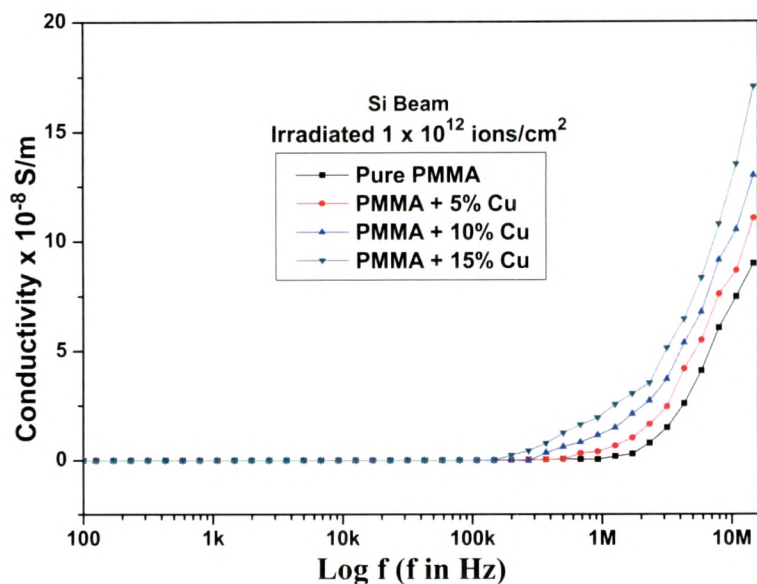
(b)



(c)



(d)



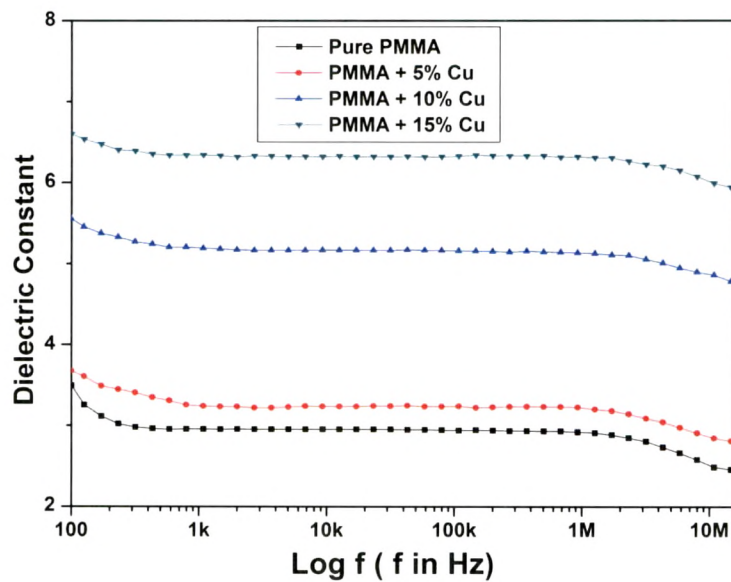
(e)

**Fig. 4.5 Conductivity Vs Log f for (a) pristine (b) C beam ( $1 \times 10^{11}$  ions/cm<sup>2</sup>) (c) C beam ( $1 \times 10^{12}$  ions/cm<sup>2</sup>) (d) Si beam ( $1 \times 10^{11}$  ions/cm<sup>2</sup>) (e) Si beam ( $1 \times 10^{12}$  ions/cm<sup>2</sup>)**

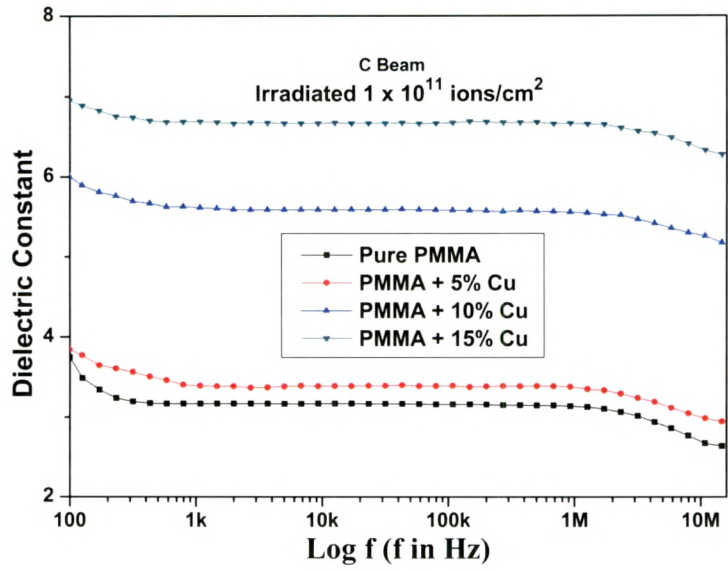
*Dielectric properties of composites:*

The variation of dielectric constant with respect to frequency for the PMMA/ copper nano composites at different filler concentrations are shown in Figure 4.6 (a -e). The dielectric constant depends on the filler concentration and irradiation fluence. Due to doping of copper nanoparticles, the quantity of the accumulated charge increases because of polarization of the polymer/metal at interfaces. The polarization makes an additional contribution to the charge quantity. From this point of view, the dielectric constant of the composites will be higher than the pure polymer. Permittivity is a frequency dependent parameter in polymer/polymer composites systems. All the free dipolar functional groups in the polymer chain can orient themselves resulting in a higher permittivity value at lower frequencies. The slow migration of the active species may be the cause of decrease in the dispersion at higher frequencies.

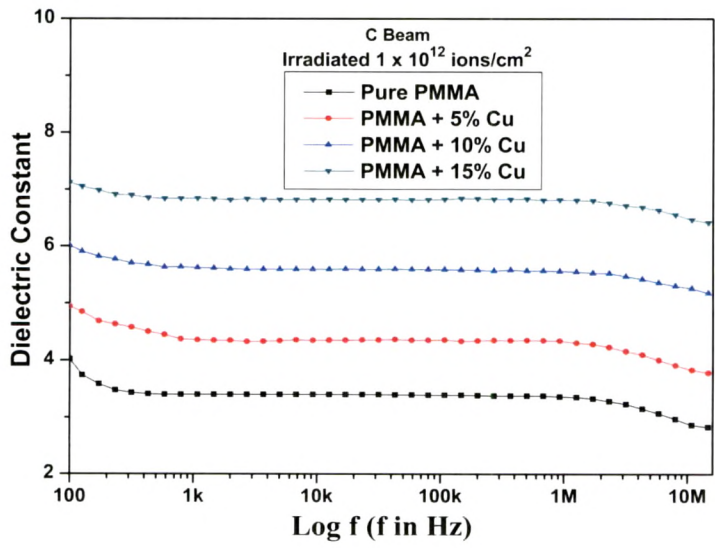
Commonly at low frequency region, the variation of dielectric constant with frequency suggests the presence of higher space charge polarizability of the material. The dielectric constant is found to decrease with increasing frequency. In the direction of applied field, the electronic exchange of the number of ions provides local displacements of electrons which produce the polarization in the polymeric composites. This gradually decreasing dielectric constant with increased frequency is thought to be caused by the slow dielectric relaxation of the matrix and the interface of the composite [27-29].



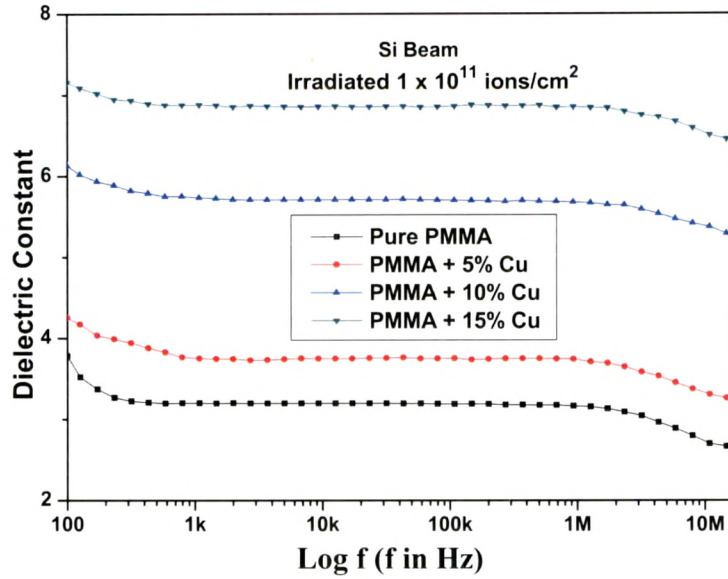
(a)



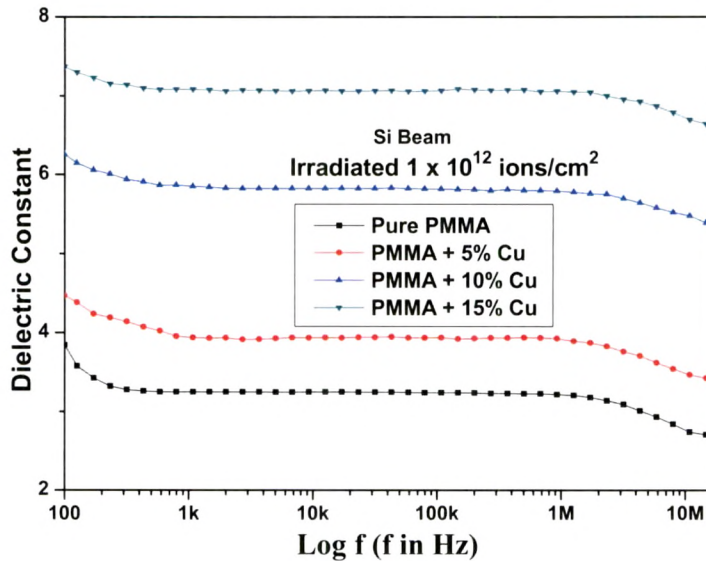
(b)



(c)



(d)

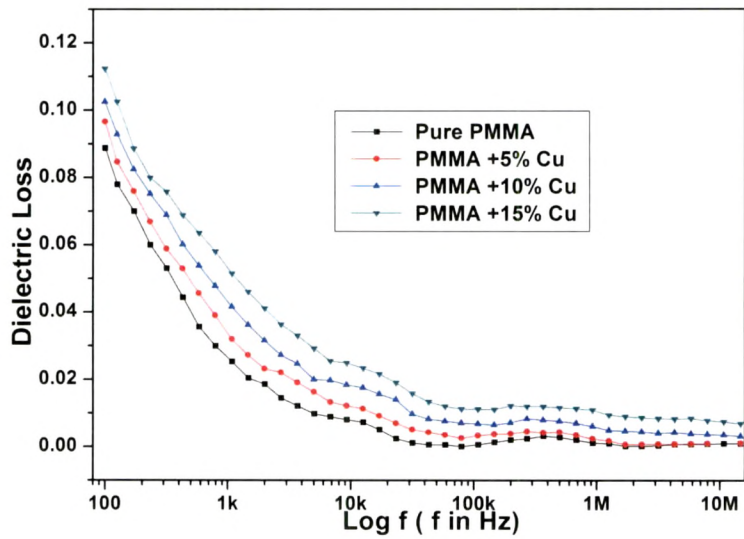


(e)

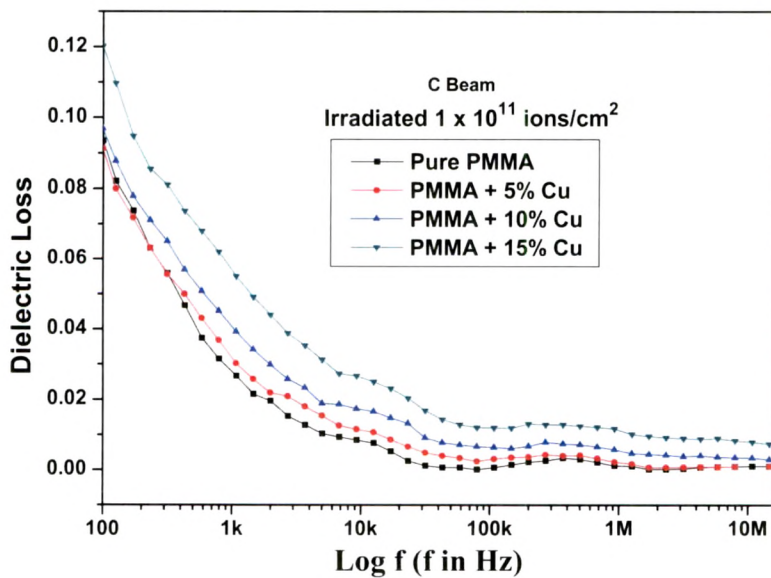
**Fig. 4.6 Dielectric constant Vs Log f for (a) pristine (b) C beam ( $1 \times 10^{11}$  ions/cm<sup>2</sup>) (c) C beam ( $1 \times 10^{12}$  ions/cm<sup>2</sup>) (d) Si beam ( $1 \times 10^{11}$  ions/cm<sup>2</sup>) (e) Si beam ( $1 \times 10^{12}$  ions/cm<sup>2</sup>)**

Fig. 4.7 (a -e) shows frequency dependence of the dielectric loss of the PMMA/Cu nano composites for pristine and irradiated samples. The dielectric loss decreased

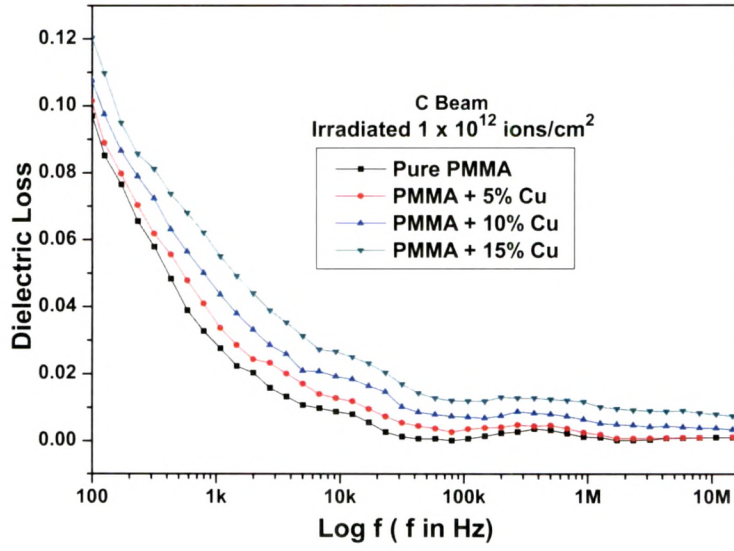
exponentially at low frequency and then became less dependent on frequency. This is because the induced charges gradually fail to follow the reversing field causing a reduction in the electronic oscillations as the frequency increased. It is noticed that dielectric loss increases moderately with the concentration of filler and also with the fluence which may be attributed to the interfacial polarization mechanism of the heterogeneous system [30, 31].



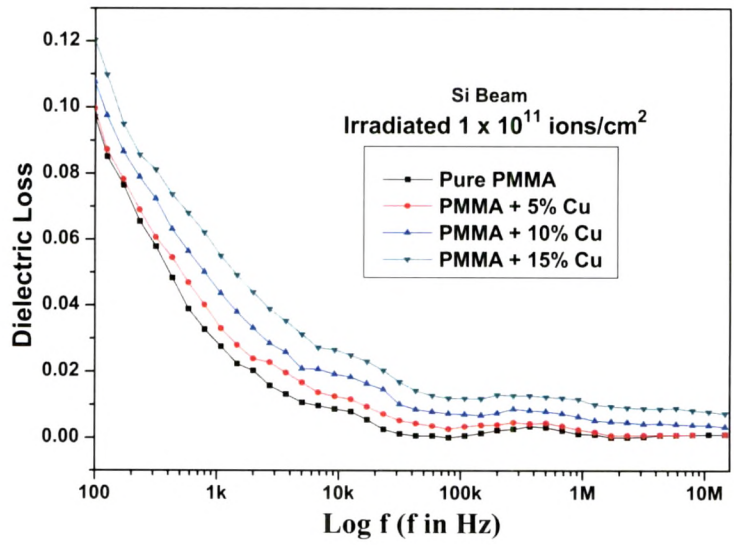
(a)



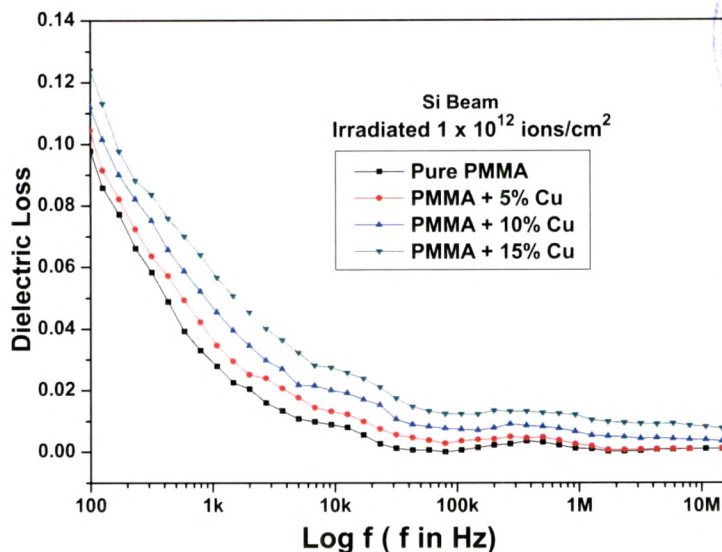
(b)



(c)



(d)



(e)

**Fig. 4.7 Dielectric loss Vs Log f for (a) pristine (b) C beam ( $1 \times 10^{11}$  ions/cm<sup>2</sup>) (c) C beam ( $1 \times 10^{12}$  ions/cm<sup>2</sup>) (d) Si beam ( $1 \times 10^{11}$  ions/cm<sup>2</sup>) (e) Si beam ( $1 \times 10^{12}$  ions/cm<sup>2</sup>)**

**Conclusion:**

Dispersion of copper nanoparticles in PMMA films has enhanced the properties of the pure polymer significantly. The increase in dielectric properties with different concentrations may be pointed to the conductive phase formed by dispersed nanoparticles in polymer matrix. Ion beam irradiation also has been shown to significantly enhance the dielectric properties may be due to conversion of the polymeric structure into a hydrogen-depleted carbon network. It was found that the band gap value moved to lower energy (from 4.30 eV upto 3.22 eV) on doping with copper nanoparticles as well as upon irradiation as observed from the UV- visible spectroscopy analysis. An XRD analysis reveals that the crystallite size of the samples decreased after ion beam irradiation which is also corroborated with the DSC analysis due to the chain scissioning upon irradiation.

## 4.2 Effect of swift heavy ions irradiation on PS + Cu nanocomposites:

### 4.2.1 X-ray diffraction analysis:

The X-ray diffraction patterns of pristine and irradiated Cu nanocomposites are shown in Fig. 4.8. It clearly indicates that copper is a crystalline but polymer is amorphous in nature and its composites show semi-crystalline behaviour. The diffraction patterns of the irradiated samples by 85 MeV C ions and 120 MeV Si ions which exhibited an increase in the peak intensity and a decrease in the full width at half maximum (FWHM) corresponding to all observed peaks of copper. This behavior may be attributed to cross-linking effect, which may results in the alignment of the polymeric chains.

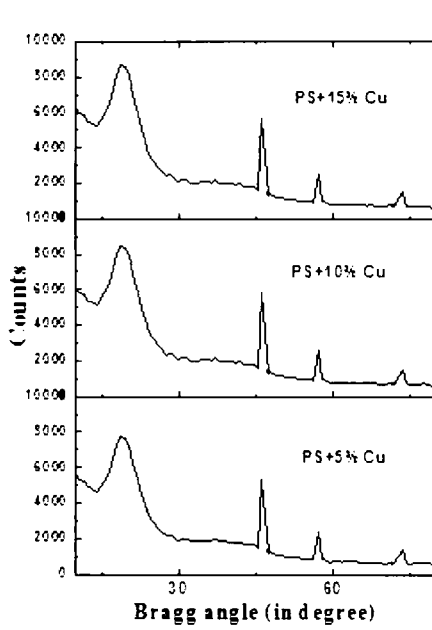
**Table 4.4 Crystallite size of pristine and irradiated samples**

Sample	Pristine		C Beam		Si Beam	
	2 $\theta$	Crystallite size (nm)	Crystallite size (nm) (1x10 <sup>11</sup> ) ions/cm <sup>2</sup>	Crystallite size (nm) (1x10 <sup>12</sup> ) ions/cm <sup>2</sup>	Crystallite size (nm) (1x10 <sup>11</sup> ) ions/cm <sup>2</sup>	Crystallite size (nm) (1x10 <sup>12</sup> ) ions/cm <sup>2</sup>
PS+ 5%Cu	46.13	11.67	11.74	11.86	12.06	12.21
	57.22	11.94	12.07	12.14	12.20	12.38
	Average	11.80	11.90	12.00	12.13	12.29
PS + 10%Cu	46.16	11.78	11.88	11.96	12.08	12.36
	57.25	12.02	12.11	12.34	12.16	12.58
	Average	11.90	11.99	12.15	12.12	12.47
PS + 15%Cu	46.18	11.89	11.98	12.98	13.21	13.52
	57.23	12.06	12.25	13.11	13.29	13.78
	Average	11.97	12.11	13.05	13.25	13.65

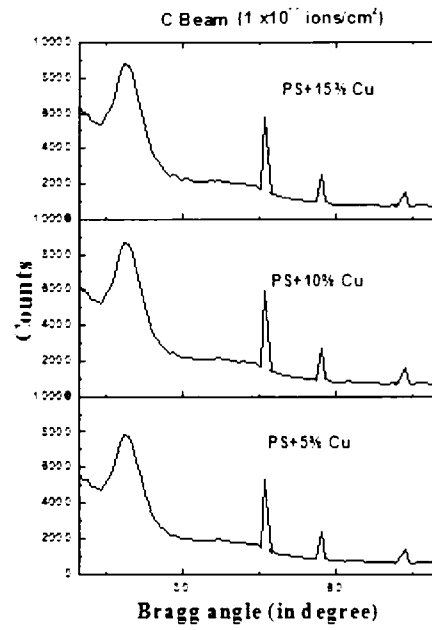
The average crystallite size ( $t$ ) for pristine and irradiated samples was calculated using Scherrer's formula [11] as given in the chapter 2 in section 2.3.1 by relation 2.2.3.

$$b = K\lambda / L \cos\theta$$

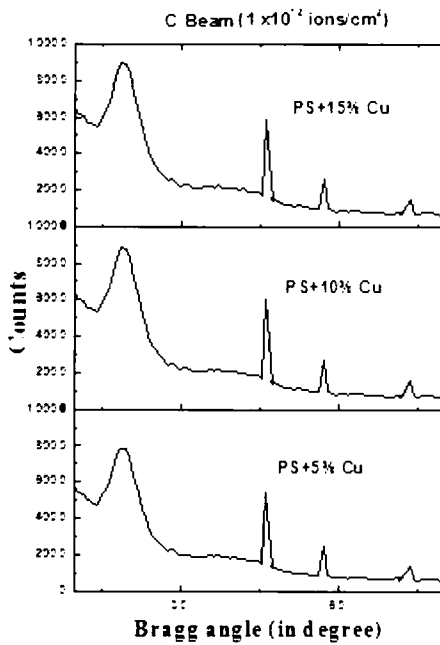
where  $b$  is FWHM in radians,  $\lambda$  is the wavelength of X-ray beam (1.5418 Å),  $L$  is the crystallite size in Å,  $K$  is a constant which varies from 0.89 to 1.39, but for most of the cases it is close to 1.



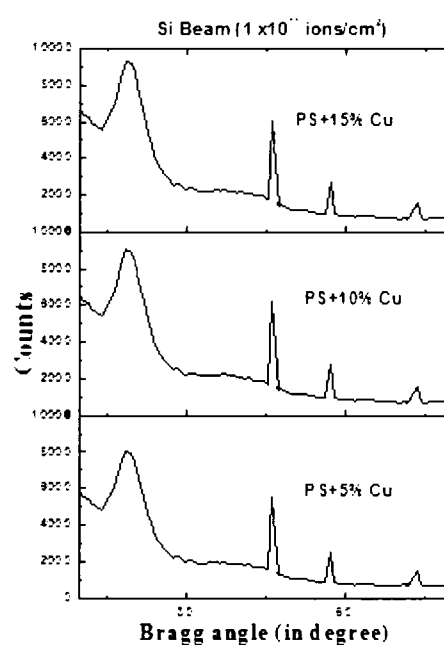
(a)



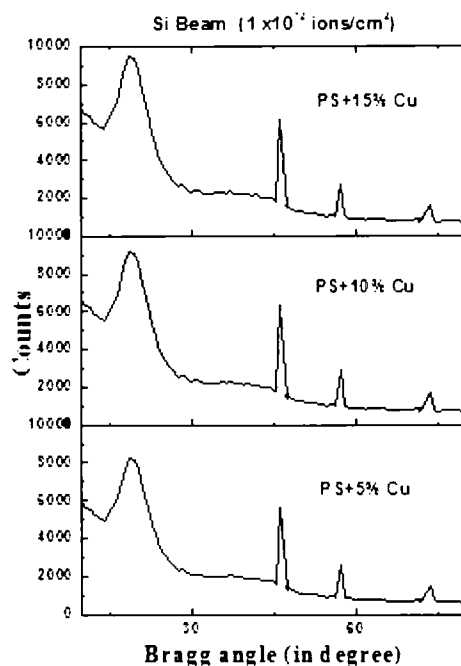
(b)



(c)



(d)



(e)

**Fig 4.8 X-ray diffraction patterns of (a) PS+ Cu (pristine) (b) C beam ( $1 \times 10^{11}$  ions/cm<sup>2</sup>) (c) C beam ( $1 \times 10^{12}$  ions/cm<sup>2</sup>) (d) Si beam ( $1 \times 10^{11}$  ions/cm<sup>2</sup>) (e) Si beam ( $1 \times 10^{12}$  ions/cm<sup>2</sup>)**

The crystallite size was calculated corresponding to the peak of the pristine and irradiated samples and the results are listed in Table 4.4. The increase in crystallite size suggested the cross linking mechanism [32].

#### **4.2.2 Thermal response (Differential scanning calorimetry (DSC)):**

The glass transition temperature ( $T_g$ ) is an important physical parameter to characterize the structural property of an amorphous polymer in terms of chain rigidity and intermolecular forces [30]. The interaction of polymer chains and nanoparticles surfaces can alter the chain kinetics by decreasing or increasing glass transition temperature of the polymer.  $T_g$  of the pure PS is observed at 66.2 °C and of that compositess are ahown in Fig 4.9. The value of  $T_g$  at highest fluence is listed in Table 4.5. Also, it should be pointed out that increase of

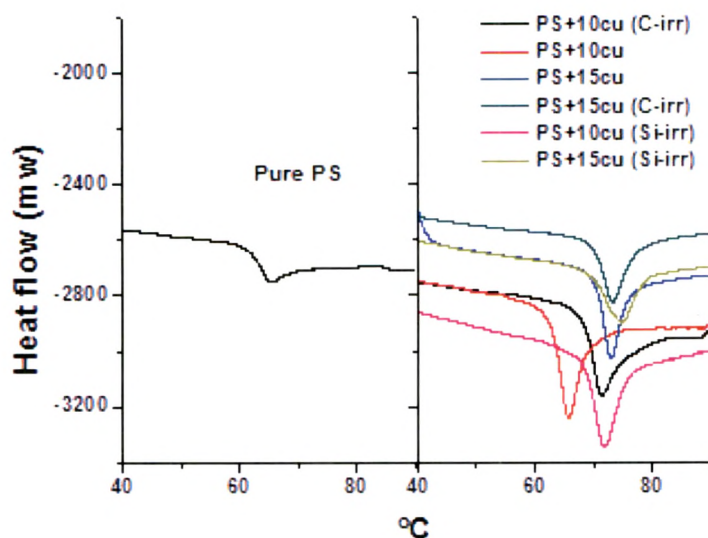


**Fig. 4.9 DSC spectra of pure, composites and irradiated ( $1 \times 10^{12}$  ions/cm<sup>2</sup>) films**

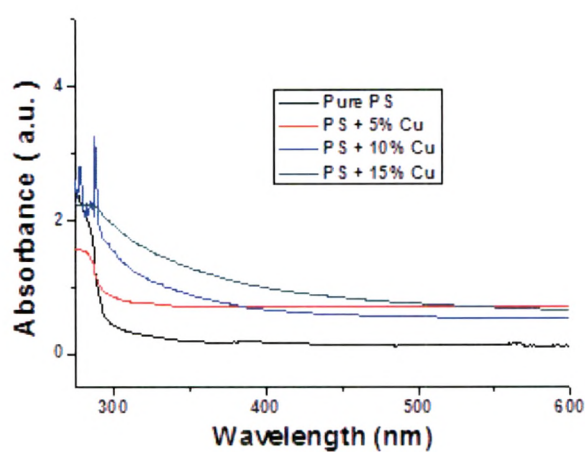
**Table 4.5 Values of glass transition for pristine and irradiated composites**

Sample name	Tg (Pristine)	Tg (C beam)	Tg (Si beam)
PS + 10 %Cu	65.9	71.4	72.2
PS + 15 %Cu	72.9	73.3	74.8

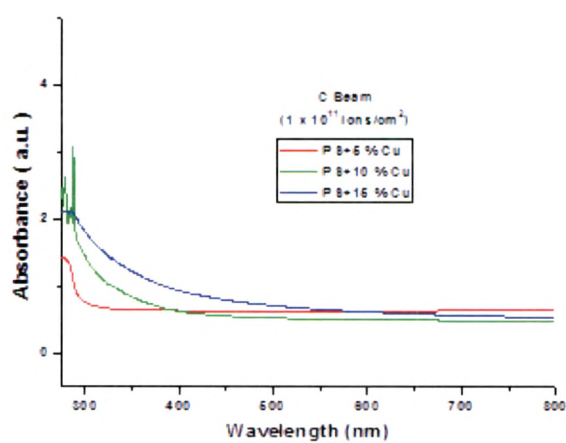
Tg with the increase of energy loss as well as with filler content indicates that the mobility of the matrix is altered due to decrease of the interparticle distances. This result is in agreement with previous DSC measurements of Bergeret and Alberola [33]. So after irradiation with ions, glass transition temperature is shifted further towards higher temperature, this further reveals cross linking between nanoparticles and polymer matrix which is also corroborated with XRD results. This behavior probably arises due to branching formed (cross linking effect) when islands of nanoparticles are bonded with polymeric chains. This lowers the mobility of the chains, and as a result the glass transition temperature increases in the nanocomposites [34].

### **4.2.3 Optical response:**

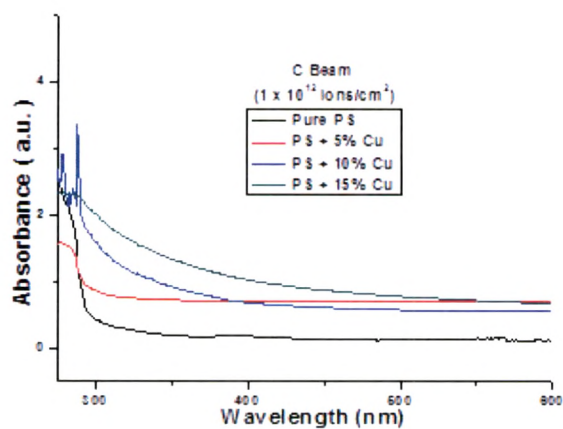
UV-vis spectroscopy is an important tool to investigate the value of optical band gap energy ( $E_g$ ). The electronic transitions ( $\rightarrow$ ) that are involved in the ultraviolet and visible regions are of the following type  $\sigma \rightarrow \sigma^*$ ,  $n \rightarrow \pi^*$ , and  $\pi \rightarrow \pi^*$  [35]. The absorbance edge of the UV-vis spectra of pristine nanocomposites and irradiated by C ions and Si ions shown in Fig 4.10 (a-e). The absorbance in aromatic compounds is due to the  $\pi$  to  $\pi^*$  transition. This is very sensitive to the change in the environment around the phenyl ring [36]. It is observed that optical absorption increases with increasing energy loss and this absorption shifts from UV-vis to the visible region for all irradiated nanocomposite samples. With increase of electronic energy loss, the nanocomposites become gradually opaque to the visible light and the absorption edge shifted from UV to the visible. This is consistent with the observation that the material changes from transparent to opaque with increase of energy deposition. The increase in absorption with irradiation may be attributed to the formation of a conjugated system of bonds due to bond cleavage and reconstruction [37]. The shifting of absorption edge towards visible is generally considered to result from carbonization of the material under irradiation [38] which is also corroborated with dielectric results.



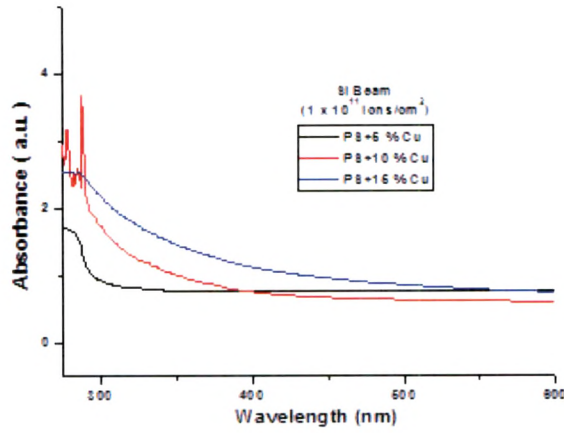
(a)



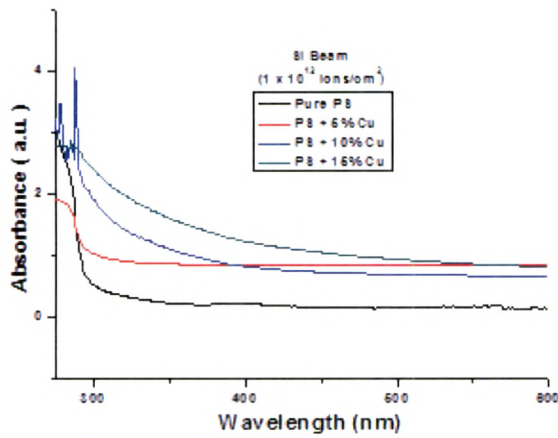
(b)



(c)



(d)



(e)

**Fig. 4.10 Absorbance spectra for (a) PS+ Cu( pristine), (b) C beam ( $1 \times 10^{11}$  ions/cm<sup>2</sup>) (c) C beam ( $1 \times 10^{12}$  ions/cm<sup>2</sup>) (d) Si beam ( $1 \times 10^{11}$  ions/cm<sup>2</sup>) (e) Si beam ( $1 \times 10^{12}$  ions/cm<sup>2</sup>)**

***Determination of optical band gap:***

Optical feature of the pristine and irradiated samples have been studied by Perkin-Elmer 25 Lambda UV-Visible spectroscope in the frequency range 200-800 cm<sup>-1</sup> as

illustrated in Fig. 4.10(a-e). The optical band gap  $E_g$  is obtained by Tauc's equation [17].

$$\text{i. e. } \omega\varepsilon(\lambda) = (\hbar\omega - E_g)^2$$

Where  $\varepsilon(\lambda)$  is the optical absorbance and  $\lambda$  is the wavelength. The intersection of the extrapolated spectrum with the abscissa of the plot  $\varepsilon^{1/2}/\lambda$  versus  $1/\lambda$  yields the gap wavelength  $\lambda_g$  from which the energy gap is derived as  $E_g = hc/\lambda_g$ . It is noticed that the band gap (energy gap) value shifted to lower energy from 4.33 eV upto 3.40 eV due to doping of copper nanoparticles and also upon irradiation of both ions. This behavior of the optical gap of ion-irradiated samples can be explained following the model of Robertson and O Reilly [39, 40].

The number of carbon hexagon rings in the cluster (M) is then found from the relation [40]

$$E_g \approx 2 |\beta| \sqrt{M}$$

Where,  $|\beta|$  is a bond integral that represents the interaction energy of two  $\pi$  atomic orbitals. A theoretical value for  $|\beta|$  proposed by Robertson and O Reilly is 2.9 eV, which according to Compagnini et al. [28] is an overestimation of the true value. So, the best-fit value of  $|\beta|$  given by them is 2.2 eV. In the present study on the aromatic polymer, given equation has been used to calculate the value of M and its behaviour with different ions is summarized in Table 4.6. The number of rings (M) remains constant with the filler and upon irradiation except for Si-ions at a fluence of  $1 \times 10^{12}$  ions/cm<sup>2</sup>.

**Table 4.6 Band gap by direct allowed transitions, number of carbon atoms in pure PS, composites and irradiated films.**

Sample	Pristine		C Beam		Si Beam	
	Band gap in eV	No. of carbon hexagon rings	Band gap in eV	No. of carbon hexagon rings	Band gap in eV	No. of carbon hexagon rings
PS + 5%Cu (1 x 10 <sup>11</sup> ions/cm <sup>2</sup> )	4.33	~1	4.28	~1	4.04	~1
PS + 5%Cu (1 x 10 <sup>12</sup> ions/cm <sup>2</sup> )	4.30	~1	3.94	~1	3.88	~1
PS + 10%Cu (1 x 10 <sup>11</sup> ions/cm <sup>2</sup> )	4.24	~1	3.90	~1	3.78	~1
PS + 10%Cu(1 x 10 <sup>12</sup> ions/cm <sup>2</sup> )	4.17	~1	3.82	~1	3.60	~1
PS + 15%Cu (1 x 10 <sup>11</sup> ions/cm <sup>2</sup> )	4.10	~1	3.75	~1	3.50	~1
PS + 15%Cu(1 x 10 <sup>12</sup> ions/cm <sup>2</sup> )	3.98	~1	3.65	~1	3.40	~2

#### **4.2.4 Surface morphology:**

Fig. 4.11(a–c) shows the SEM images of pristine, composites and irradiated composite films with magnification of X250. The analysis shows that the filled particles are distributed randomly in the matrix which display continuous contact between themselves and formed conducting paths. The surface becomes smoothen upon irradiation. The decrease in roughness with Cu-nanoparticles may be attributed to the decrease in density of metal particles on the surfaces of the films, which is also responsible for increase in crystallinity of the material as indicated by XRD analysis.

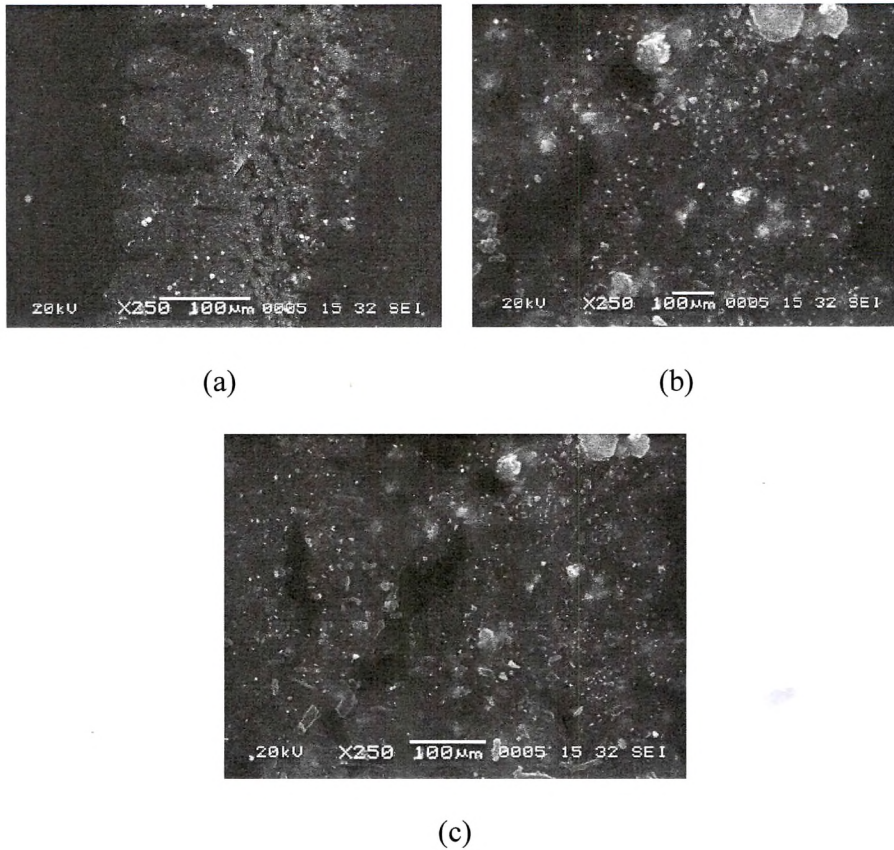
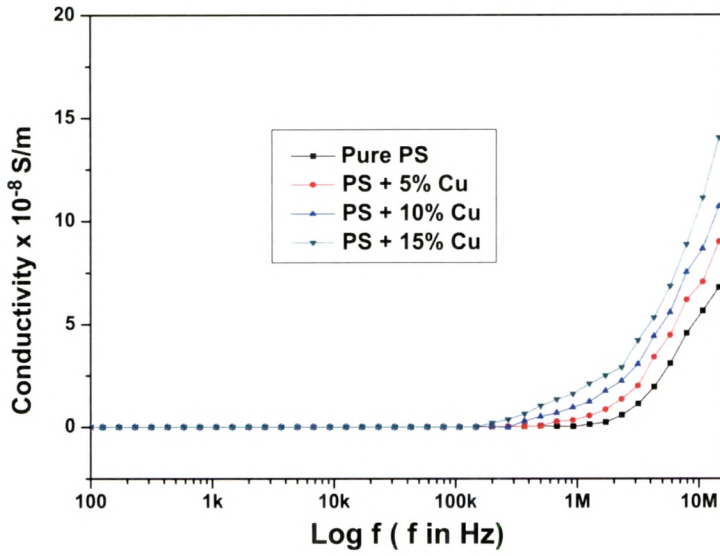


**Fig. 4.11 SEM images of (a) PS+ 15 % Cu (pristine) (b) PS + 15 % Cu (C beam-  $1 \times 10^{12}$ ) (c) PS + 15 % Cu (Si beam-  $1 \times 10^{12}$ )**

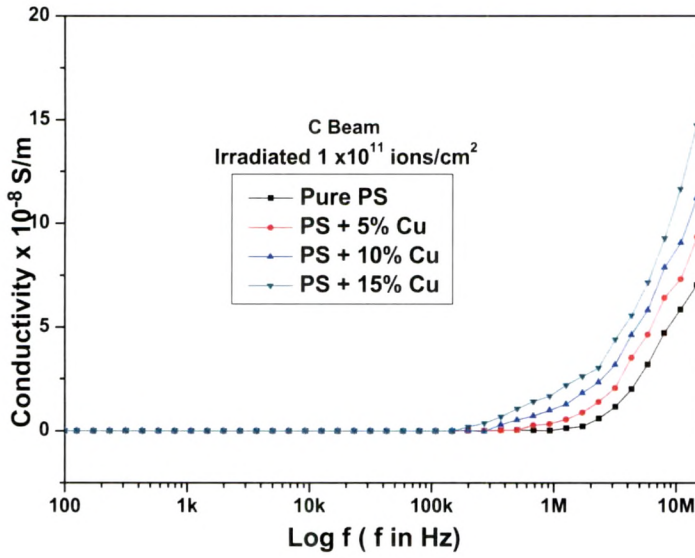
#### ***4.2.5 AC electrical frequency response:***

*Conductivity:* The ac conductivity of the composites as a function of the frequency is shown in the Fig.4.12 (a-e). The conductivity of composite was studied with respect to irradiation fluence and filler concentration. The conductivity of composite was increased with concentration of filler that is possibly due to the electronic interaction process taking place in the composites and therefore resulted composites show more conductive with the increase of the filler content [41]. It is known that the electrical conductivity of such composites depends on the type and concentration of the fillers. Irradiation is expected to promote the metal to polymer bonding and convert the polymeric structure into a hydrogen depleted carbon network due to emission of

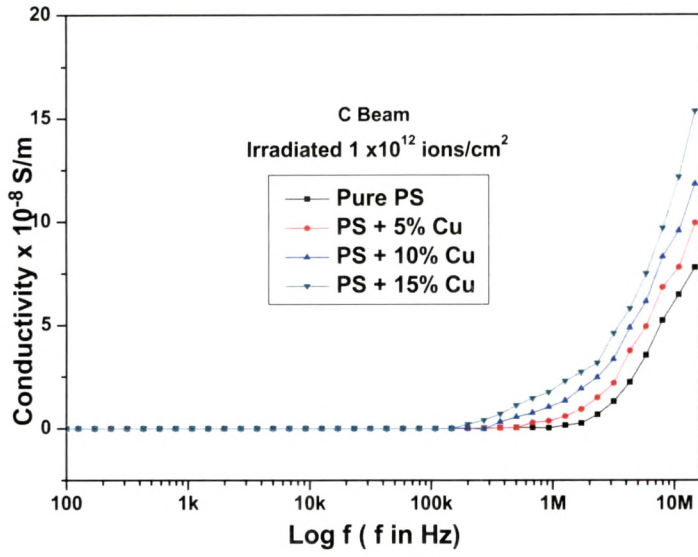
hydrogen and/or other volatile gases. It is this carbon network that is believed to make the polymer more conductive [32].



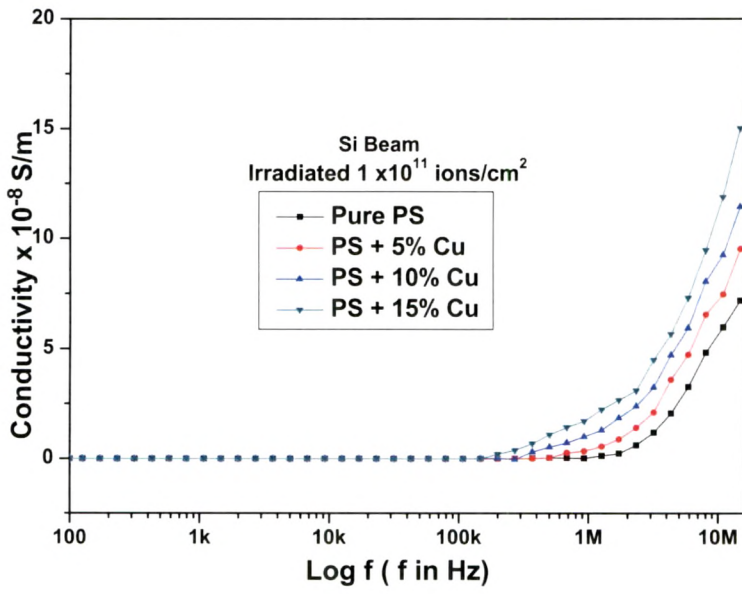
(a)



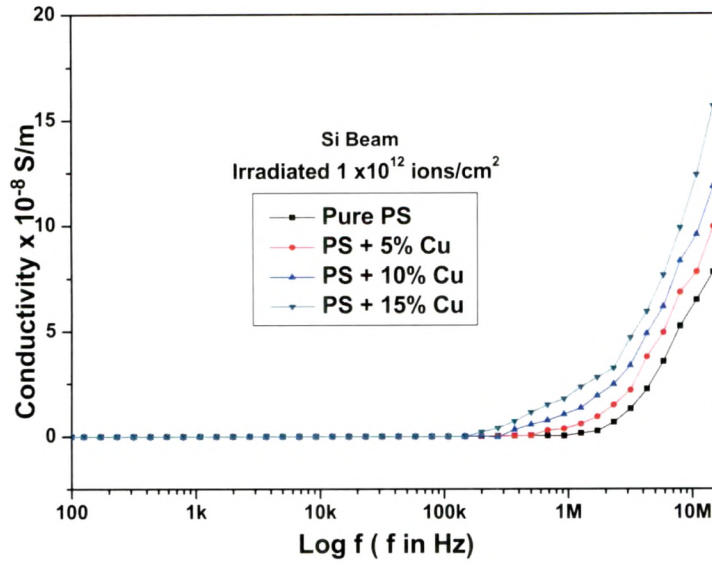
(b)



(c)



(d)

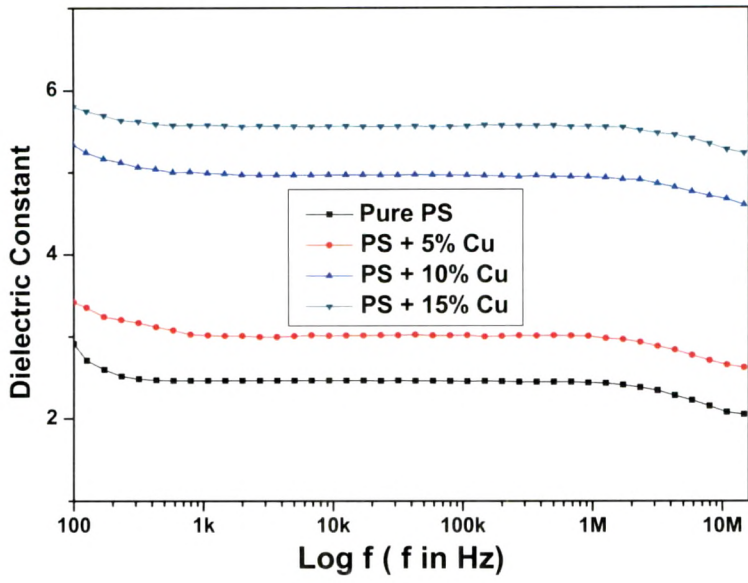


(e)

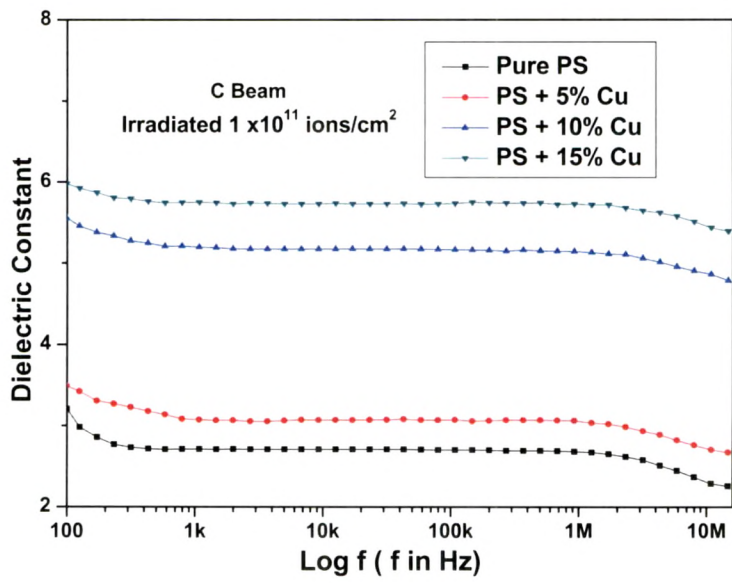
**Fig. 4.12 Conductivity Vs Log f for (a) pristine (b) C beam ( $1 \times 10^{11}$  ions/cm<sup>2</sup>) (c) C beam ( $1 \times 10^{12}$  ions/cm<sup>2</sup>) (d) Si beam ( $1 \times 10^{11}$  ions/cm<sup>2</sup>) (e) Si beam ( $1 \times 10^{12}$  ions/cm<sup>2</sup>)**

*Dielectric properties of composites:*

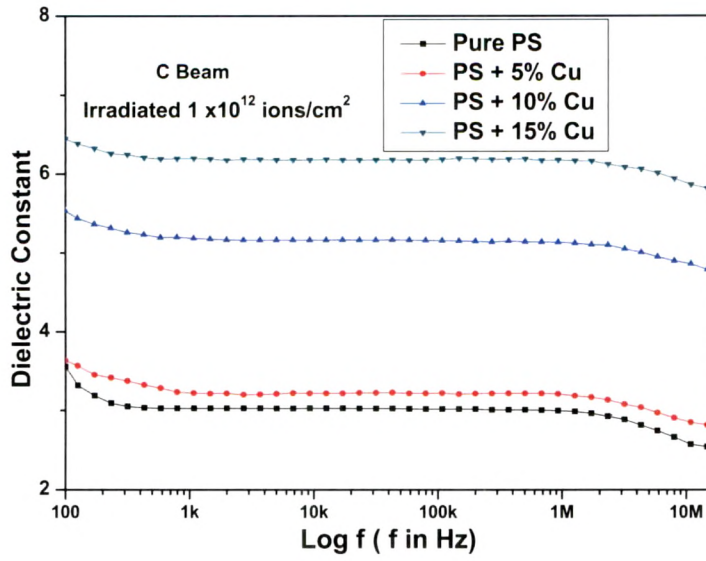
Fig. 4.13 (a-e) shows the variation of dielectric constant of pristine and irradiated PS/Cu nanocomposites at different concentrations (5%, 10%, 15%) of Cu nanoparticles as a function of frequency with C-ions and Si-ions respectively. The increase in the dielectric content with filler content is a direct consequence of interfacial polarization effect between polymer and the filler particles [42, 43]. It is observed that dielectric permittivity remains almost constant up to 100 kHz, because the motion of charge carriers is almost constant at these frequencies. As frequency increases further the polarization of trapped and bound charges cannot take place due to the charge carriers migrate through the dielectric and get trapped against defect sites and induces an opposite charge in its vicinity and hence the dielectric constant



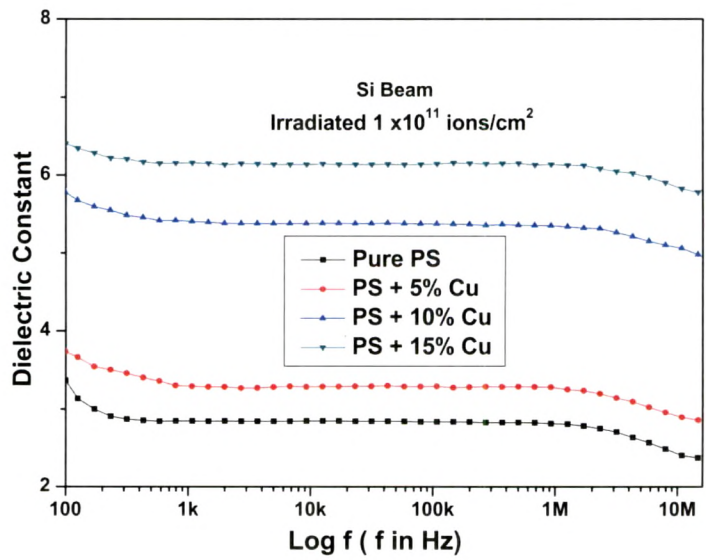
(a)



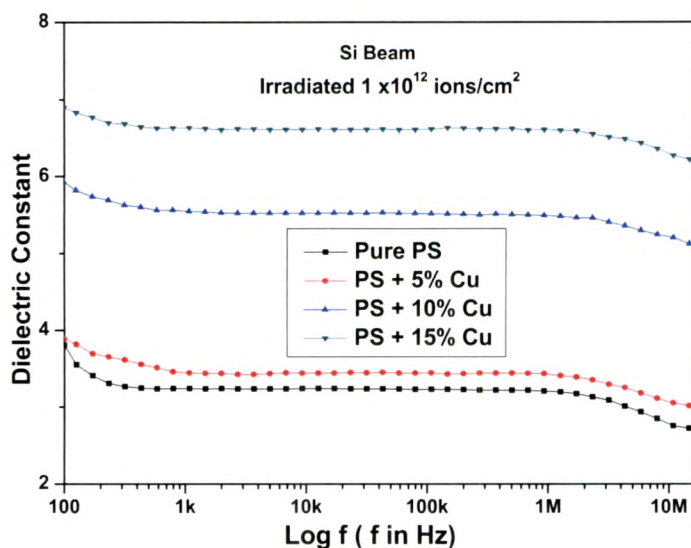
(b)



(c)



(d)



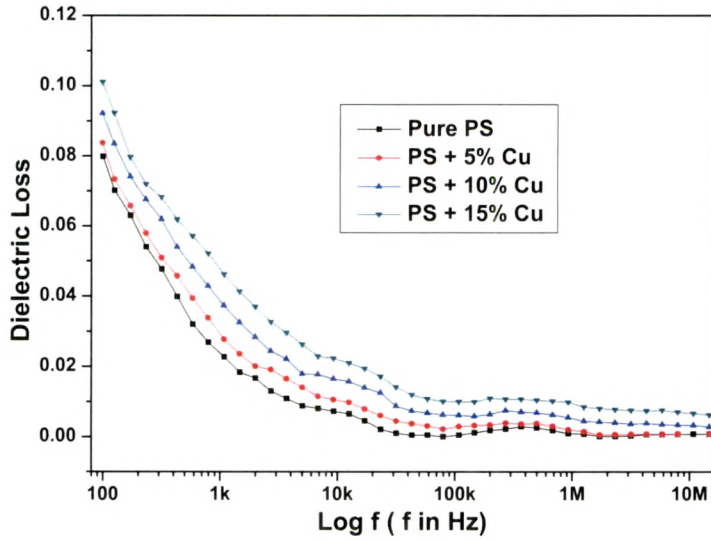
(e)

**Fig. 4.13 Dielectric Constant Vs Log f for (a) pristine (b) C beam ( $1 \times 10^{11}$  ions/cm<sup>2</sup>) (c) C beam ( $1 \times 10^{12}$  ions/cm<sup>2</sup>) (d) Si beam ( $1 \times 10^{11}$  ions/cm<sup>2</sup>) (e) Si beam ( $1 \times 10^{12}$  ions/cm<sup>2</sup>)**

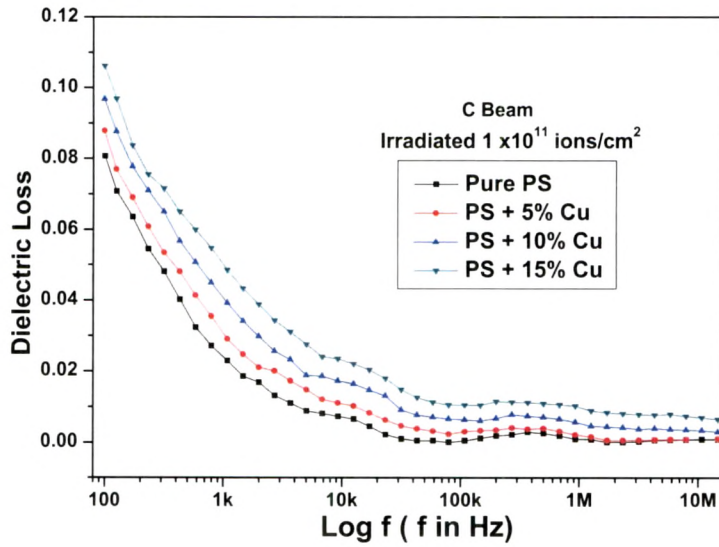
decreases. Also according to Dissado and Hill theory at high frequency, intra-cluster motions are dominant. In intra-cluster motions, the relaxation of a dipole will produce a ‘chain’ response in its neighboring dipoles and the reaction of the neighboring dipoles will, in turn, affect the first dipole, so the overall effect will be seen as a single cluster dipole moment relaxation [30, 44]. This reduces the dielectric constant at these frequencies. It was also observed that dielectric constant increases after ion beam irradiation by both ions (C and Si) which may be attributed to chain scission and the resulting an increase in free radicals, unsaturation etc.

The increase in dielectric loss with increasing filler contents may be attributed to the interfacial polarization mechanism of the heterogeneous system. Fig. 4.14 (a-e) shows the variation of dielectric loss with frequency of pristine and irradiated with C-ion and Si-ion respectively. The dielectric loss decreases exponentially and then becomes less dependent on frequency. This is because the induced charges gradually fail to follow

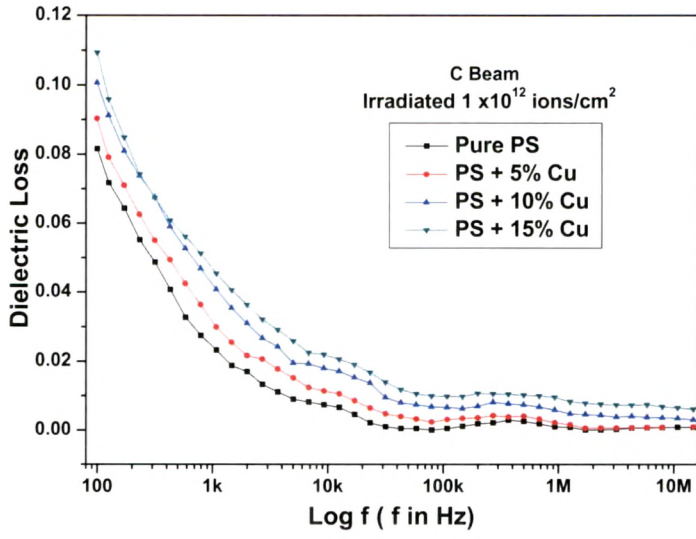
the reversing field, causing a reduction in the electronic oscillations as frequency increases [30].



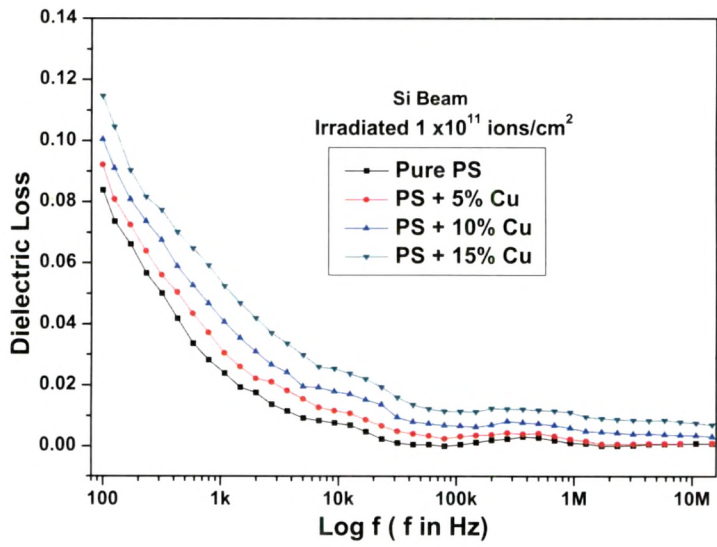
(a)



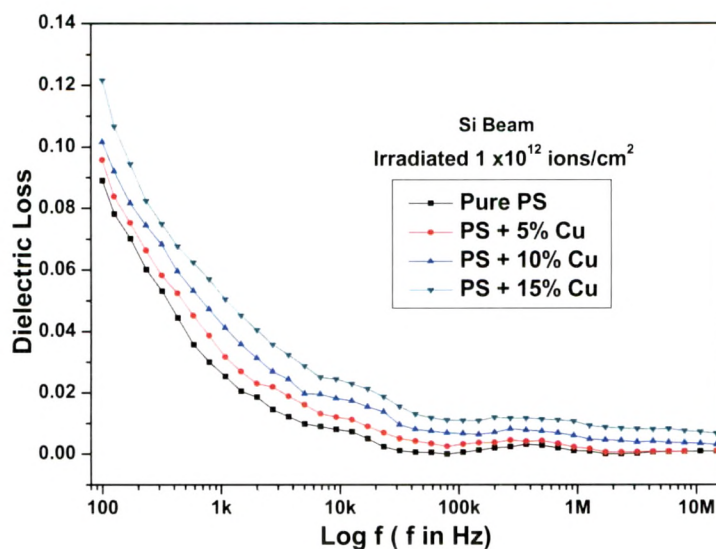
(b)



(c)



(d)



(e)

**Fig. 4.15 Dielectric loss Vs Log f for (a) pristine (b) C beam ( $1 \times 10^{11}$  ions/cm<sup>2</sup>) (c) C beam ( $1 \times 10^{12}$  ions/cm<sup>2</sup>) (d) Si beam ( $1 \times 10^{11}$  ions/cm<sup>2</sup>) (e) Si beam ( $1 \times 10^{12}$  ions/cm<sup>2</sup>)**

**Conclusion:**

Dispersion of copper nanoparticles in PS films has enhanced the properties of the pure polymer significantly. An XRD analysis reveals that the crystallite size of the samples increased after ion beam irradiation which is also corroborated with the DSC analysis due to the cross linking effect upon irradiation. It is found that the band gap value moved to lower energy (from 4.33 eV upto 3.40 eV) on doping with copper nanoparticles as well as upon irradiation as observed from the UV- visible spectroscopy analysis. The increase in dielectric properties with different concentrations may be pointed to the conductive phase formed by dispersed nanoparticles in polymer matrix. Ion beam irradiation also has been shown to significantly enhance the dielectric properties may be due to conversion of the polymeric structure into a hydrogen-depleted carbon network. So we have concluded that effect of Si-beam is more effective than that of the C-beam in the present study because of large energy loss of heavy ion.

### 4.3 Summary

In this chapter, two different nano composites i.e (PMMA/Cu, PS/Cu) have been studied using two different ions beams (C and Si) irradiations. Structural, optical, thermal, electrical properties and surface morphology have been examined by different characterization techniques.

XRD analysis; In PMMA/Cu nanocomposites, results show that the crystallite size of fillers decreases slightly upon both ions beams irradiations as observed from XRD analysis. It is also observed that the intensity of the peak decreases and to some extent broadening of the peak after irradiation offers confirmation of decrease in crystallinity. Since no significant change in the peak position is observed, this reveals that lattice parameters do not change significantly in both ions irradiations. Whereas in the case of PS nanocomposites, crystallite size of fillers increases upon both ions irradiations which may be attributed to cross linking phenomenon.

DSC thermograms; the T<sub>g</sub> value decreases upon irradiations in PMMA nanocomposites and increases upon irradiations in PS composites. This behavior probably arises due to branching (cross-linking effect) when islands of nanoparticles are bonded with polymeric chains. This lowers the mobility of the chains, and as a result, the glass transition temperature increases in the nanocomposites.

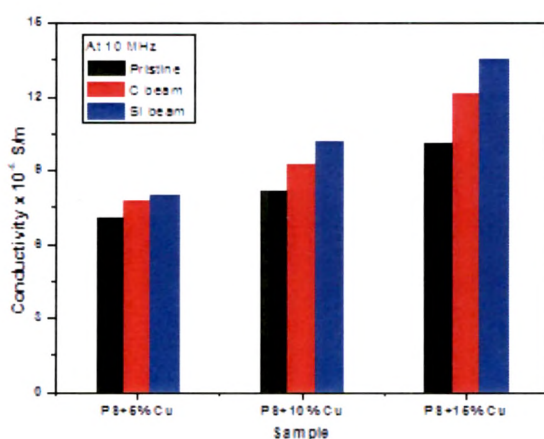
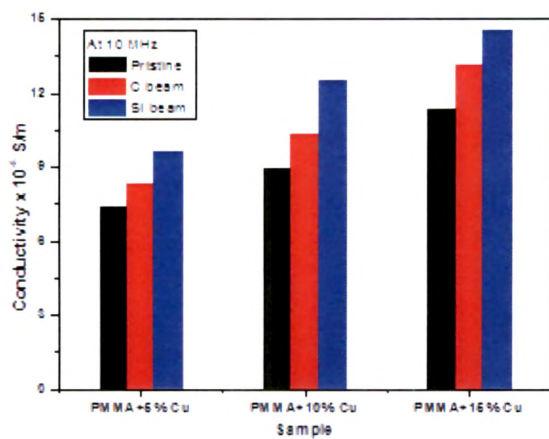
UV-Vis analysis; the band gap values for both composites were increased upon concentration of fillers and both ions irradiations. It was observed from the UV-visible spectroscopy analysis that the band gap value moved to the lower energy.

Surface morphology; SEM images showed that increase in density in PMMA nanocomposites and decrease in density in PS nanocomposites upon irradiations.

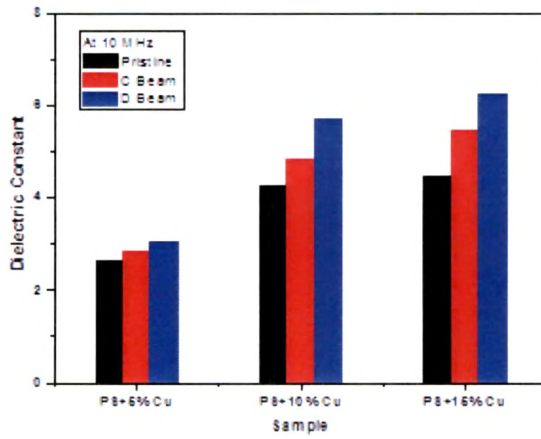
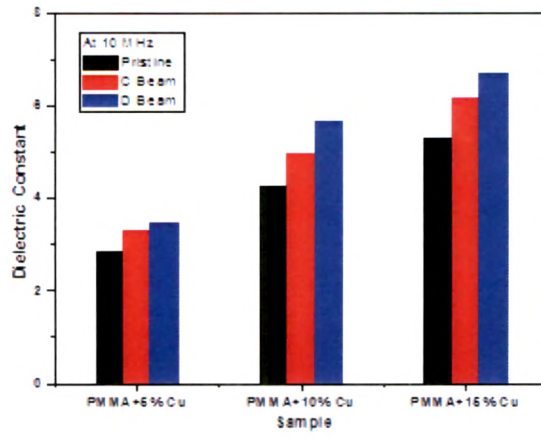
Dielectric analysis; Ac electrical conductivity of all pristine and irradiated samples at different filler concentrations is shown in Fig.4.16. The increase in conductivity with copper nanoparticles concentration for pristine samples may be attributed to the conductive phase formed by dispersed metal nanoparticles in polymer matrix. The conductivity of composite was studied with respect to irradiation fluence and filler concentration. The conductivity of composite was increased with concentration of filler that is possibly due to the electronic interaction process taking place in the composites and therefore resulted composites show more conductive with the increase of the filler content. It is known that the electrical conductivity of such composites depends on the type and concentration of the fillers. Irradiation is expected to promote the metal to polymer bonding and convert the polymeric structure into a hydrogen depleted carbon network due to emission of hydrogen and/or other volatile gases. It is this carbon network that is believed to make the polymer more conductive Fig 4.16 shows comparison of conductivity of all composites before and after irradiation. For the sake of comparison filler concentration (5, 10, 15 wt%) at a fluence of  $1 \times 10^{12}$  ions/cm<sup>2</sup> for C and Si ions beam at a frequency 10 MHz have considered. In Fig 4.17, shows similar comparison for dielectric constant of all composites.

Fig.4.17 shows the dependence of the dielectric constant on the frequency of the applied field at different filler concentrations and irradiation fluences.

In all the cases, it reveals that dielectric loss is positive and signifies inductive behaviour of the material.



**Fig. 4.16 Comparison of Conductivity of pristine and irradiated samples at 10 MHz**



**Fig. 4.17 Comparison of Dielectric constant of pristine and irradiated samples at 10 MHz**

References:

- [1] J.L. Wilson, P. Poddar, N.A. Frey, H. Srikanth, K. Mohamed, J.P. Harmon, S. Kotha, J. Wachsmuth, *J. Appl. Phys.* 95 (2004) 1934.
- [2] A. Heilmann, *Polymer Films with Embedded Metal Nanoparticle*, Springer, New York, 2003.
- [3] P. O' Rourke Muisener, L. Clayton, J. D' Angelo, J.P. Harmon, *J. Mater. Res.* 17 (2002) 2507.
- [4] H. Qiao, Z. Wei, H. Yang, L. Zhu, X. Yan, *J. Nanomater.* 2009 (2009) 795928.
- [5] H. Gleiter, *Progr. Mater. Sci.* 33 (1990) 223.
- [6] Z.L. Wang, Y. Liu, Z. Zhang, *Handbook of Nanophase and Nanostructured Materials*, Tsinghua University Press, Beijing, China, 2002.
- [7] G. H. Chan, J. Zhao, E. M. Hicks, G. C. Schatz, R. P. V. Duyne, *Nano letters* 7(7) (2007) 1947.
- [8] Z. Zhu, C. Liu, Y. Sun, J. Liu, Y. Yang, Y. Jin, J. Du, *Nucl. Instrum. Methods B* 191 (2002) 723.
- [9] Chaitali Gavade, Sangeeta Kishorea, N.L. Singh, P.K. Khanna, *Radiation Effects and Defects in Solids*, 168 (2013) 504.
- [10] Chaitali Gavade, N. L. Singh, P. K. Khanna , Sunil Shah, *Journal of nanoscience and nanotechnology*. (communicated)
- [11] P. Scherrer, *Gott Nachr* 2 (1918) 98–100.
- [12] A. K. Srivastava, H. S. Virk, *J. Polym. Mater.* 17 (2000) 325.

- [13] N. L. Singh, D. Singh, A. Qureshi, *Radiation Effects & Defects in Solids* 66(8-9) (2011) 640–647.
- [14] A. Semwal, A. Negi, R. G. Sonkawade, J. M. S. Rana, R. C. Ramola, *Indian J of pure and App Phy* 48 (2010) 496-499.
- [15] H S Virk , P S Chandi And A K Srivastava, *Bull. Mater. Sci.* 24(5) (2001) 529.
- [16] L. Singh, K. Singh Samra, *Radiation Physics and Chemistry* 77 (2008) 252–258.
- [17] A. Das, S. Dhara and A. Patnaik *Physical Rev B* 59 (1999) 11069.
- [18] Anjum Qureshi , Dolly Singh , N.L. Singh, S. Ataoglu , Arif N. Gulluoglu , Ambuj Tripathi ,D.K. Avasthi, *Nuclear Instruments and Methods in Physics Research B* 267 (2009) 3456.
- [19] S. Shah, N.L. Singh, A. Qureshi, D. Singh, K.P. Singh, V. Shrinet, A. Tripathi, *Nucl. Instrum. Methods B* 226 (2008) 1768.
- [20] N. L. Singh, A. Qureshi, A. K. Rakshit, D. K. Avasthi, *Bull. Mater. Sci.*,29 (2006) 605-609.
- [21] M. Abu-Abdeen, G. M. Nasr, H. M. Osman, A. I. Abound, *Egypt. J. Sol.*, 25 (2002) 275-294.
- [22] Y. P. Mamunya, V. V. Davyadenko, P. Pissis, E. V. Lebedev, *Eur. Polym. J.*,28 (2002) 1887-1897.
- [23] D. Singh, N. L. Singh, A. Qureshi, P. Kulriya, A. Tripathi, D. K. Avasthi, A. N. Gulluoglu, *J. Non-Cryst. Solids*, 356 (2010) 856-863.
- [24] S. M. Reda, *Dyes and Pigments*,75 (2007) 526-532.
- [25] S. Shah, N. L. Singh, A. Qureshi, D. Singh, K. P. Singh, V. Shrinet, A. Tripathi, *Nucl. Instrum. Methods B* 226 (2008) 1768-1774.
- [26] Y. Q. Wang, M. Curry, E. Tavenner, N. Dobson, R. E. Giedd, *Nucl. Instrum.*

Methods B 219 (2004) 798-803.

[27] S. Prasher, M. Kumar, S. Singh, Asian Journal of Chemistry, 21(10) (2009) S043-S046.

[28] S. Singh, M. Thomas Joy, IEEE Transactions on Dielectrics and Electrical Insulation, 2008, 15(1).

[29] G. Sui, S. Jana, W. H. Zhong, M.A. Fuqua, C. A. Ulven, Acta Materialia, 56 (2008) 2381–2388.

[30] N. L. Singh, S. Shah, A. Qureshi, K. P. Singh, V. Shrinet, P. K. Kulriya, A. Tripathi, Radiation Effects & Defects in Solids, 163(2) (2008) 169-177.

[31] N. L. Singh, S. Shah, A. Qureshi, A. Tripathi, F. Singh, D. K. Avasthi, P. M. Raole, Bull. Mater. Sci., 34(1) (2011) 81–88.

[32] D. Singh, N.L. Singh, A. Qureshi, P. Kulriya, A. Tripathi, D.K. Avasthi, A.N. Gulluoglu, J. Non-Cryst. Solids, 356 (2010) 856–863.

[33] A. Qureshi, N. L. Singh, S. Shah, F. Singh, D.K. Avasthi, J. Macromol. Sci., 45 (2008) 265–270.

[34] S. Shah, D. Singh, A. Qureshi, N. L. Singh, K. P. Singh, V. Shrinet, Indian J. Pure Appl. Phys., 46 (2008) 439–442.

[35] Rajesh Kumar, S. Asad Ali, A.K. Mahur, H.S. Virk, F. Singh, S.A. Khan, D.K. Avasthi, Rajendra Prasad, Nuclear Instruments and Methods in Physics Research B 266 (2008) 1788–1792.

[36] S. Saravanana, M.R. Anantharaman, S. Venkatachalam, D.K. Avasthi, Vacuum 82 (2008) 56–60.

[37] L.S. Farenza, R.M. Papaleo, A. Hallen, M.A. Araujo, R.P. Livi, B.U.R. Sundqvist, Nucl. Instr. and Meth. B 105 (1995) 134.

- [38] Zhiyong Zhu, Yunfan Jin, Changlong Liu, Youmei Sun, Mingdong Hou, Chonghong Zhang, Zhiguang Wang, Jie Liu, Xiaoxi Chen, Baoquan Li, Yanbin Wang, *Nuclear Instruments and Methods in Physics Research B* 169 (2000) 83-88.
- [39] J. Robertson, E.P. O Reilly, *Phys. Rev. B* 35 (1987) 2946.
- [40] Lakhwant Singh, Kawaljeet Singh Samra, Ravinder Singh, *Nuclear Instruments and Methods in Physics Research B* 255 (2007) 350–356.
- [41] Z. Elimat, *J. Phys. D: Appl. Phys.*, 39 (2006) 2824-2828.
- [42] Anjum Qureshi, Ayhan Mergen, Mehmet S. Eroglu, N. L. Singh, Arif Gu Lluoglu, *Journal of Macromolecular Science, Part A: Pure and Applied Chemistry* 45 (2008) 462–469.
- [43] G.C. Psarras, E.Manolakaki, G.M. Tsangarris, *Composites A* 33 (2002) 375-384.
- [44] L.A. Dissado and R.M. Hill, *Proc. Roy. Soc. London* 390 (1983) 131.